# Supporting Information

# Elucidating reaction pathway of decarboxylation-assisted olefination catalyzed by a mononuclear non-heme iron enzyme

Chen-Ping Yu, Yijie Tang, Lide Cha, Sergey Milikisiyants, Tatyana I. Smirnova, Alex I. Smirnov, Yisong Guo, Wei-chen Chang

*Department of Chemistry, North Carolina State University, Raleigh, NC 27695. Department of Chemistry, Carnegie Mellon University, Pittsburgh, PA 15213.*

**Contents:**

## General

All reagents were used directly as obtained from the commercial sources. The relative molecular mass and purity of enzyme samples were determined using SDS-polyacrylamide gel electrophoresis (SDS-PAGE). The protein molecular weight marker used was purchased from Fisher Bioreagents (EZ-Run$^{TM}$ Protein Marker). NMR spectra were recorded on a Bruker 300, 400 or 700 MHz spectrometer. Chemical shifts ($\delta$ in ppm) are given relative to that of solvent ($CDCl_3$, $D_2O$, and $CD_3OD$), with coupling constants (*J*) reported in Hertz (Hz). Analytical thin layer chromatography (TLC) was carried out on pre-coated TLC aluminum plate (silica gel, grade 60, $F_{254}$, 0.25 mm layer thickness) acquired from EMD Chemicals (Gibbstown, NJ). Flash column chromatography was performed using silica gel (230-400 mesh, grade 60) obtained from Sorbent Technologies. Liquid Chromatography-Mass Spectrometry (LC-MS) were carried out on Agilent 1200 series LC system connected to a single quadruple mass spectrometer, Agilent 6120 (Agilent Technologies).

## Preparation of compound 1

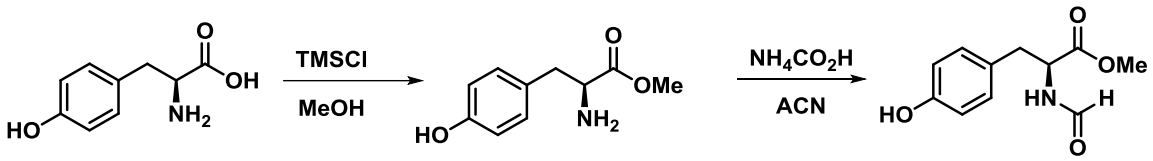


**Methyl formyl-L-tyrosinate.** To a stirred solution of L-tyrosine (502 mg, 2.77 mmol) in methanol (MeOH, 9.3 mL) was added trimethylsiyl chloride (TMSCl, 1.2 mL, 9.46 mmol) at 0 $^oC$ slowly. After addition, the reaction mixture was kept stirring at room temperature overnight. Subsequently, the solvent was removed under reduced pressure and the crude residue was used directly in the next step without purification.

Ammonium formate (700 mg, 11.09 mmol) was added into a acetonitrile solution (ACN, 9.3 mL) containing crude product at room temperature and the reaction was brought to reflux until no starting material was detected by TLC (ethyl acetate/hexanes = 4/1 (v/v), $R_f$ = 0.45). After cooling down to room temperature, the reaction mixture was filtered and the filtrate was concentrated under reduced pressure. The crude product was purified by silica gel column chromatography (ethyl acetate/hexanes = 2/1 (v/v)) to give the product (537 mg, 87%); $^1H$ NMR (400 MHz, $CD_3OD$) $\delta$ 8.02 (s, 1H), 7.00 (d, *J* = 8.4 Hz, 2H), 6.70 (d, *J* = 8.4 Hz, 2H), 4.70 (dd, *J*

= 8.0, 5.6 Hz, 1H), 3.70 (s, 3H), 3.04 (dd, *J* = 14.0, 5.6 Hz, 1H), 2.90 (dd, *J* = 14.0, 8.0 Hz, 1H). (Fig. S1)

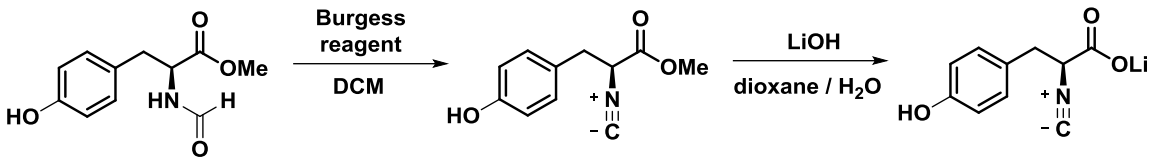


**Compound 1**. To a stirred solution of methyl formyl-L-tyrosinate (532 mg, 2.38 mmol) in dichloromethane (DCM, 8.0 mL) was added Burgess reagent (858 mg, 3.60 mmol) at room temperature. After addition, the mixture was brought to reflux until no starting material can be detected by TLC (ethyl acetate/hexanes = 1/1 (v/v), $R_f$ = 0.53, ~ 2 hours). The solvent was removed under reduced pressure, then the reaction mixture was purified by silica gel column chromatography (ethyl acetate/hexanes = 1/2 (v/v)) to give the product (188 mg, 38%); $^1$H NMR (400 MHz, $CDCl_3$) δ 7.10 (d, *J* =8.6 Hz, 2H), 6.79 (d, *J* = 8.8 Hz, 2H), 5.57 (broad s, 1H), 4.43 (dd, *J* = 8.0, 4.8 Hz, 1H), 3.80 (s, 3H), 3.18 (dd, *J* = 14.0, 4.8 Hz, 1H), 3.08 (dd, *J* = 14.0, 8.0 Hz, 1H); $^{13}$C NMR (100 MHz, $CDCl_3$) δ 166.6, 159.8, 155.5, 130.5, 126.0, 115.7, 58.3, 53.4, 38.1. (Fig. S2)

Next, the saponification was carried out to obtain compound **1**. To a stirred solution of methyl ester (152 mg, 0.74 mmol) in dioxane/$H_2O$ = 2:1 (total of 2.5 mL) was added lithium hydroxide monohydrate (LiOH•$H_2O$, 48 mg, 1.14 mmol) at room temperature. The mixture was stirred at room temperature for 1 hour and the solvent was removed *in vacuo* to give the final product **1** (141 mg, 97%); $^1$H NMR (400 MHz, $D_2O$) δ 7.04 (d, *J* =8.4 Hz, 2H), 6.59 (d, *J* = 8.4 Hz, 2H), 4.34 (dd, *J* = 8.0, 4.4 Hz, 1H), 3.03 (dd, *J* = 14.0, 4.4 Hz, 1H), 2.90 (dd, *J* = 14.0, 8.0 Hz, 1H); $^{13}$C NMR (100 MHz, $D_2O$ ) δ 173.2, 163.3, 152.9 (t, *J* = 6.8 Hz, isocyananide carbon), 130.6, 122.7, 118.0, 61.2 (t, *J* = 6.7 Hz, α-carbon), 37.8. The $^{13}$C NMR was obtained using relaxation delay of $T_1$ = 4 seconds. (Fig. S3)

Compound D-**1** was synthesized via the identical procedure using corresponding L-tyrosine-3,3-$d_2$ as the starting material.

**Preparation of compounds 3, 4 and 5.** Compound **3**, **4** and **5** were prepared analogously using L-phenylalanine, L-4-fluoro-phenylalanine, and L-4-trifluoromethyl-phenylalanine as the starting material. The NMR characterization is as listed.

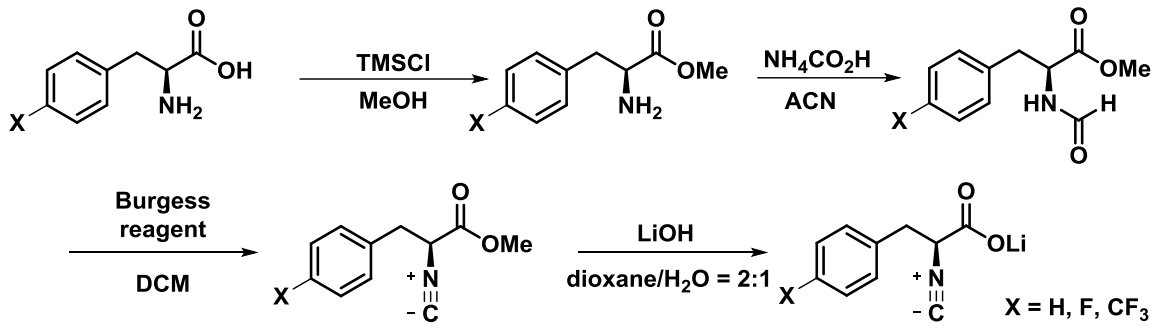


Methyl formyl-L-phenylalaninate (95% yield over two steps). $^1$H NMR (400 MHz, $CDCl_3$) δ 8.14 (s, 1H), 7.30-7.24 (m, 3H), 7.13-7.10 (m, 2H), 6.26 (broad s, 1H), 4.96 (dd, *J* = 6.0, 14.0 Hz, 1H), 3.74 (s, 3H), 3.14 (m, 2H). (Fig. S4)

Methyl (*S*)-2-isocyano-3-phenylpropanoate (53% yield). $^1$H NMR (400 MHz, $CDCl_3$) δ 7.38-7.31 (m, 3H), 7.27-7.25 (m, 2H),4.47 (dd, *J* = 8.4, 4.8 Hz, 1H), 3.80 (s, 3H), 3.26 (dd, *J* = 14.0, 4.8 Hz, 1H), 3.14 (dd, *J* = 14.0, 8.4 Hz, 1H); $^{13}$C NMR (100 MHz, $CDCl_3$) δ 166.3, 160.7, 134.2, 129.1, 128.6, 127.6, 57.8, 53.1, 38.6. (Fig. S5)

Compound **3** (99% yield). $^1$H NMR (400 MHz, $D_2O$) δ 7.40-7.36 (m, 2H), 7.35-7.32 (m, 3H), 4.46 (dd, *J* = 6.0, 6.0 Hz, 1H), 3.19 (broad d, *J* = 13.6 Hz), 3.08 (dd, *J* = 15.6, 6.0 Hz, 1H); $^{13}$C NMR (100 MHz, $D_2O$) δ 172.7, 153.2 (t, *J* = 6.8 Hz, isocyananide carbon), 136.1, 129.4, 128.5, 127.3, 60.7 (t, *J* = 7.0 Hz, α-carbon), 38.4. (Fig. S6)

Methyl formyl-L-4-furoro-phenylalaninate (78% yield over two steps). $^1$H NMR (300 MHz, $CDCl_3$) δ 8.19 (s, 1H), 7.09-6.95 (m, 4H), 6.08 (broad s, 1H), 4.95 (m, 1H), 3.75 (s, 3H), 3.17 (dd, *J* = 14.1, 6.0 Hz, 1H), 3.10 (dd, *J* = 14.1, 5.7 Hz, 1H). (Fig. S7)

Methyl (*S*)-2-isocyano-3-(4-fluoro-phenyl)propanoate (61% yield). $^1$H NMR (400 MHz, $CDCl_3$) δ 7.23-7.20 (m, 2H), 7.06-7.00 (m, 2H), 4.45 (dd, *J* = 8.0, 4.8 Hz, 1H), 3.77 (s, 3H), 3.22 (dd, *J* = 14.0, 4.8 Hz, 1H), 3.11 (dd, *J* = 14.0, 8.0 Hz, 1H); $^{13}$C NMR (100 MHz, $CDCl_3$) δ 166.2, 162.3 (d, *J* = 244.8 Hz), 161.1, 130.8 (d, *J* = 8.1 Hz), 130.0 (d, *J* = 3.3 Hz), 115.5 (d, *J* = 21.5 Hz), 57.8, 53.2, 37.8. (Fig. S8)

Compound **4** (99% yield).$^1$H NMR (700 MHz, $D_2O$) δ 7.32 (m, 2H), 7.11 (m, 2H), 4.49 (m, 1H), 3.18 ( broad d, *J* = 13.3 Hz, 1H), 3.12 (broad s, 1H); $^{13}$C NMR (100 MHz, $D_2O$) δ 172.4, 161.7

(d, *J* = 241.3 Hz), 153.2 (t, *J* = 7.5 Hz, isocyananide carbon), 131.7 (d, *J* = 3.0 Hz), 130.9 (d, *J* = 8.2 Hz), 115.0 (d, *J* = 21.3 Hz), 60.6 (t, *J* = 6.4 Hz, α-carbon), 37.4. (Fig. S9)

Methyl formyl-L-4-trifuromethyl-phenylalaninate (61% yield over two steps). $^{1}$H NMR (300 MHz, $CDCl_3$) δ 8.17 (s, 1H), 7.54 (d, *J* = 8.0 Hz, 2H), 7.23 (d, *J* = 8.0 Hz, 2H), 6.21 (broad s, 1H), 4.98 (m, 1H), 3.75 (s, 3H), 3.26 (dd, *J* = 13.8, 6.0 Hz, 1H), 3.16 (dd, *J* = 13.8, 5.7 Hz, 1H). (Fig. S10)

Methyl (*S*)-2-isocyano-3-(4-(trifluoromethyl)phenyl)propanoate (38% yield). $^{1}$H NMR (400 MHz, $CDCl_3$) δ 7.60 (d, *J* = 7.9 Hz, 2H), 7.38 (d, *J* = 8.2 Hz, 2H), 4.52 (dd, *J* = 8.2, 4.8 Hz, 1H), 3.79 (s, 3H), 3.31 (dd, *J* = 14.0, 4.8 Hz, 1H), 3.20 (dd, *J* = 14.0, 8.2 Hz, 1H); $^{13}$C NMR (100 MHz, $CDCl_3$) δ 166.0, 161.4 (broad s), 138.3, 130.0 (q, *J* = 33.4 Hz), 129.7, 125.6 (q, *J* = 3.7 Hz), 123.9 (q, *J* = 270.4 Hz), 57.3 (broad s), 53.3, 38.2. (Fig. S11)

Compound **5** (89% yield). $^{1}$H NMR (700 MHz, $D_2O$) δ 7.69 (d, *J* = 5.6 Hz, 2H), 7.48 (d, *J* = 5.6, 2H), 4.53 (broad s, 1H), 3.28 (broad d, *J* = 3.5 Hz, 1H), 3.18 (broad s, 1H); $^{13}$C NMR (175 MHz, $D_2O$) δ 172.3, 153.6, (t, *J* = 6.3 Hz, isocyananide carbon), 140.3, 129.9, 128.7 (q, J = 31.9 Hz), 125.3 (broad s), 124.3 (q, *J* = 269.5 Hz), 60.4 (t, *J* = 6.5 Hz, α-carbon), 38.1. (Fig. S12)

**Preparation of compounds 2, 6, 7, 8 and diethyl (isocyanomethyl)phosphonate.**

**Preparation of diethyl (isocyanomethyl)phosphonate.** Due to current unavailability of diethyl (isocyanomethyl)phosphonate, it was synthesized with in a five-step sequence with overall 12% yield.

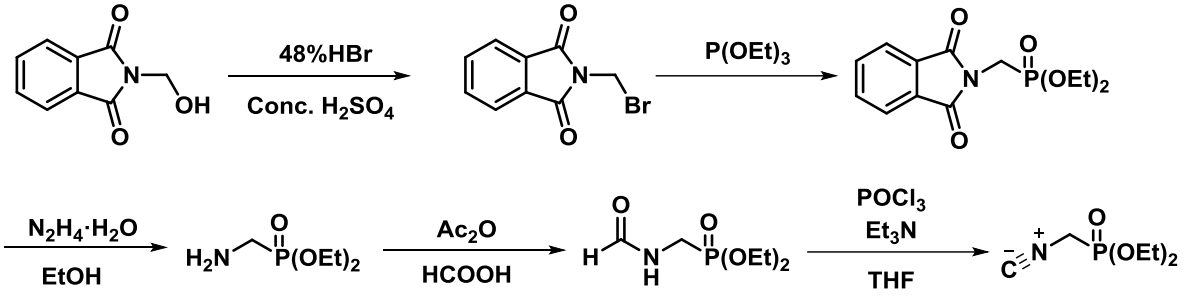


To a mixture of *N*-hydroxymethylphthalimide (5.0 g, 28.0 mmol) and 48% aqueous hydrobromic acid (20 mL, 1.4 M) at was added concentrated sulfuric acid (7.5 mL, 0.14 mol) with stirring over a period of 15 minutes 0 °C. Subsequently, the reaction mixture was heated at ~ 70 °C for 5 hours and then cooled overnight in a refrigerator for overnight (~0 °C, 12 hours). During this

time, the solid was precipitated and collected by suction filtration. Followed by three 20 mL portions of cold water, two 10 mL portions of cold 10% aqueous ammonium hydroxide, and three 20 mL portions of cold water, the product was dried under reduced pressure to give *N*-bromomethylphthalimide as a very l light yellow solid (96.4% yield) which was used in the next step without further purification. $^1$H NMR (300 MHz, $CDCl_3$) δ 7.92-7.95 (m, 2H), 7.78-7.81 (m, 2H), 5.49 (s, 2H). (Fig. S13)

To a stirred solution of *N*-bromophthalimide (6.53 g, 27.0 mmol) was added triethyl phosphite (5.8 mL, 34 mmol) at room temperature. After addition, the mixture was immersed in an oil bath and the temperature of the oil bath gradually increased to ~ 100 °C over 15 minutes. When the reaction has subsided (~ 14 hours), the oil bath was lowered and the condenser is removed. The flask was then fitted for simple distillation. Ethyl bromide and other volatile materials were distilled from the reaction mixture over a period of 3-4 hours by continued heating at 115°C. The resulting light-yellow oil was cooled to room temperature, whereupon it solidified. The crude product was collected by suction filtration and washed with three 25 mL portions of cold petroleum ether to give diethyl phthalimidomethylphosphonate as white crystals (90% yield), which are used in the next step without further purification. $^1$H NMR (300 MHz, $CDCl_3$) δ 7.84-7.87 (m, 2H), 7.71-7.74 (m, 2H), 4.16-4.22 (m, 4H), 4.09 (d, $J$ = 11.4 Hz, 2H), 1.32 (t, $J$ = 6.9 Hz, 6H). (Fig. S14)

To a solution of diethyl phthalimidomethylphosphonate (7.22 g, 24.3 mmol) in ethanol (100 mL) was added an ethanoic solution of hydrazine monohydrate ($N_2H_4$•$H_2O$, 1.4 mL 28.4 mmol in 5 mL EtOH) at room temperature. Subsequently, the reaction wss heated at reflux for 4 hours and then cooled to 0-5 °C in an ice bath. The precipitated phthalhydrazide was collected by suction filtration and thoroughly washed with three 25 mL portions of ethyl acetate. The excess solvents and hydrazine were removed under reduced pressure on a rotary evaporator and then under high vacuum. The crude diethyl(aminomethyl)phosphonate was directly used in the next step (78% yield). $^1$H NMR (300 MHz, $CDCl_3$) δ 4.03-4.09 (dt, $J$ = 6.9 and 3.0 Hz, 4H), 2.93 (d, $J$ = 12.0 Hz, 2H), 1.26 (t, $J$ = 6.9 Hz, 6H). (Fig. S15)

To a solution of diethyl(aminomethyl)phosphonate (3.27 g, 19.6 mmol) in formic acid was added acetic anhydride (11.8 mL, 0.13 mol) dropwise at 0°C. After addition, the reaction was warmed to room temperature and allowed for stirring for 2 hours. The reaction mixture was then diluted

with water (100 mL) and extracted with ethyl acetate (40 mL x 3). The combined organic layer was washed with saturated sodium carbonate and brine. It was dried over $MgSO_4$ and concentrated to obtain crude diethyl (formamidomethyl)phosphonate which was directly used for next step. $^1$H NMR (400 MHz, $CDCl_3$) δ 8.21 (s, 1H), 6.97(broad s, 1H), 4.19-4.07 (m, 4H), 3.72 (m, 2H), 1.32 (t, *J* = 6.8 Hz, 6H). (Fig. S16)

To a solution of diethyl (formamidomethyl)phosphonate (1.0 g, 5.1 mmol) in dry tetrahydrofuran (THF, 20 mL) was added triethylamine ($Et_3N$, 3.6 mL, 26.0 mmol) at -78 °C. The solution was stirred for 15min followed by addition of $POCl_3$ (0.5 mL, 5.6 mmol) at the same temperature. The reaction was stirred for additional 15 min at same temperature and warmed to 0°C gradually. The solution was kept stirring for 1 hour until no substrate was detected by TLC. Upon completion, the reaction was quenched by adding ice-water mixture (10 mL) and extracted with ethyl acetate (20 mL x 4). The organic layer was combined, dried, and concentrated. The residue was purified by column chromatography (ethyl acetate/hexanes = 3/1 (v/v)) to give the product (0.60 g, 3.4 mmol, with overall 12% yield). $^1$H NMR (300 MHz, $CDCl_3$) δ 4.31-4.21 (m, 4H), 3.77 (d, *J* = 15.9 Hz, 2H), 1.40 (t, *J* = 7.2 Hz, 6H); $^{13}$C NMR (75 MHz, $CDCl_3$) δ 160.5, 63.8 (d, *J* = 6.8 Hz), 37.4 (d, *J* = 155.2 Hz), 16.2 (d, *J* = 4.5 Hz); $^{31}$P NMR (121.4 MHz, $CDCl_3$) δ 13.4. (Fig. S17)

**Preparation of compounds 2.**

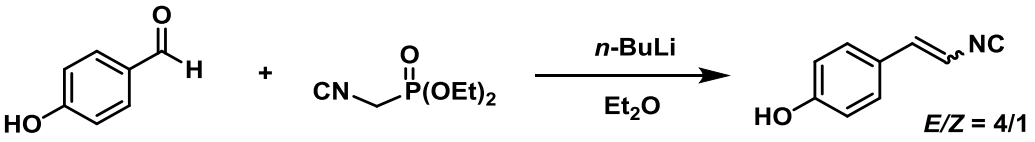


To a solution of diethyl isocyanomethyl phosphonate (170 mg, 0.96 mmol) in diethyl ether ($Et_2O$, 5.0 mL) was added *n*-BuLi (0.44 mL, 2.5 M in hexanes). After addition, the solution was stirred for 10 min at the same temperature and followed the slow addition of 4-hydroxybenzaldehyde (57 mg, 0.47 mmol) which was dissolved in 0.5 mL of $Et_2O$. The solution was stirred for 30 minutes at the same temperature and then warmed to 0 °C. The reaction was quenched by the addition of 10 % ammonium chloride aqueous solution and extracted with $Et_2O$ (5mL x 4). The organic layer was combined, dried, and concentrated. The residue was purified using neutral aluminum oxide column chromatography (diethyl ether/hexanes = 3/1) to give the product as volatile yellow oil (16% yield, with *E*/*Z* isomeric ratio of 4/1). $^1$H NMR (700 MHz,

DMSO-$d_6$) δ 10.06 (s, 0.2 H), 9.95 (s, 0.8 H), 7.63 (d, *J* = 11.9 Hz, 0.4 H), 7.39 (d, *J* = 11.9 Hz, 2H), 7.08 (d, *J* = 24.5 Hz, 1H), 6.88 (d, *J* = 11.9 Hz, 2H), 6.80 (d, *J* = 11.9 Hz, 2H), 6.72 (d, *J* = 21.7 Hz, 1H), 6.55 (d, *J* = 16.1 Hz, 1H), 6.10 (d, *J* = 12.6 Hz, 1H); $^{13}$C NMR (175 MHz, DMSO-$d_6$) δ 168.2, 163.5, 159.0, 158.8, 136.5, 131.6, 130.9, 128.7, 123.9, 123.7, 115.7, 115.7, 108.5, 106.2. (Fig. S18)

**Preparation of compounds 6, 7 and 8.** Compounds **6**, **7** and **8** were prepared in analogous manner by reacting with commercially available benzaldehydes.

Compound **6** (33% yield, *E*-isomer). $^1$H NMR (700 MHz, DMSO-$d_6$) δ 7.58-7.41(m, 5H), 7.21 (d, *J* = 14.0 Hz, 1H), 6.95 (d, *J* = 14.0 Hz, 1H); $^{13}$C NMR (175 MHz, DMSO-$d_6$) δ 164.6, 136.5, 132.8, 129.7, 128.9, 127.0, 111.7. (Fig. S19)

Compound **7** (35% yield, *E*-isomer). $^1$H NMR (700 MHz, DMSO-$d_6$) δ 7.64 (dd, *J* = 7.0, 7.0 Hz, 2H), 7.28 (dd, *J* = 7.0, 7.0 Hz, 2H), 7.22 (d, *J* = 14.0 Hz, 1H), 6.93 (d, *J* = 14.0 Hz, 1H); $^{13}$C NMR (175 MHz, DMSO-$d_6$) δ 164.6, 162.8 (d, *J* = 246.4 Hz), 135.4, 129.4, 129.3 (d, *J* = 8.8 Hz), 115.9 (d, *J* = 21.1 Hz), 112.6. (Fig. S20)

Compound **8** (33% yield, *E*-isomer). $^1$H NMR (700 MHz, DMSO-$d_6$) δ 7.78 (broad s, 4H), 7.32 (d, *J* = 14.0 Hz, 1H), 7.11 (d, *J* = 14.0 Hz, 1H); $^{13}$C NMR (175 MHz, DMSO-$d_6$) δ 165.8, 137.0, 135.1, 129.5 (q, *J* = 31.5 Hz), 127.7, 125.7, 124.0 (q, *J* = 271.3 Hz), 114.3. (Fig. S21)

**Preparation of compound 9.**

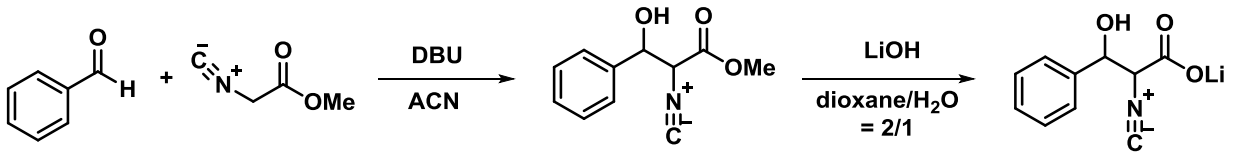


To a stirred solution of methyl 2-isocyanoacetate (170 mg, 1.71 mmol) in acetonitrile (ACN, 9.5 mL) was added 1,8-Diazabicyclo[5.4.0]undec-7-ene (DBU, 0.26 mL, 1.71 mol) at room temperature. The solution was kept stirring for 1 hour. Subsequently, a solution of benzaldehyde (205 mg, 1.94 mmol) in acetonitrile (ACN, 9.5 mL) was added dropwise to the reaction at room temperature. After addition, the solution was stirred for another 2 hours at the same temperature until no isonitrile was detected by TLC (ethyl acetate/hexanes = 1/2 (v/v), $R_f$ = 0.13). The solvent

was removed under reduced pressure and the crude residue was purified by silica gel column chromatography (ethyl acetate/hexanes = 1/2 (v/v)) to give the product (47 mg, 15%).

Next, saponification was carried out analogously as described above. To a stirred solution of substrate (37 mg, 0.18 mmol) in dioxane/$H_2O$ = 2/1 (1.8 mL) was added lithium hydroxide (LiOH, 10 mg, 0.24 mmol) at room temperature. The mixture was stirred at room temperature for 1 hour and the solvent was removed *in vacuo* to give the product **9** as a pair of stereoisomers with the ratio of ~ 6:4 (35 mg, 99%); $^1$H NMR (400 MHz, $D_2O$) δ 7.38-7.24 (m, 5 H), 5.45 (d, *J* = 7.2 Hz, 0.6H), 5.18 (broad s, 0.4 H), 4.43 (broad s, 0.4 H), 4.34 (d, *J* = 7.2 Hz, 0.6H); $^{13}$C NMR (100 MHz, $D_2O$) δ, 177.8, 175.7, 163.7, 157.1, 140.5, 139.3, 129.1, 128.9, 128.4, 127.9, 126.0, 125.8, 84.2, 76.5, 73.3, 59.4. (Fig. S22)

**DNA construct for over-expression of *P*.IsnB**

The DNA sequence encodes *p.isnB* from *P. luminescens* was codon-optimized for over-expression in *E. coli*, synthesized, and inserted into the NdeI and BamHI restriction sites of expression vector pET-28a. The codon-optimized gene sequence is shown below.

ATCATCACAGCAGCGGCCTGGTGCCGCGCGGCAGCCATATGATGACCGAACTGAATAGCTTTCA
GACCGAAGAAATTACCCCGTTTGGTCTGAAAATTACACCGCAGTATAGCGATCAGCATATTGAT
ACCCTGCCGGTTGAACAGCTGAAAGAACTGGCACGTAAACATCATCTGCTGATTCTGCGTGGTT
TTAAAAGCGATCTGAGCGATCATGAGAAATATGAGAAATACGCACGTAACTGGGGTGAAATTAT
GATGTGGCCGTTTGGTGCAATTCTGGATGTTCGTGAACATCAGGATGCAACCGATCATGTTTTT
GATAATAGCTATATGCCGCTGCATTGGGATGGTATGTATAAACCGACCATCCCGGAATTTATCA
TGTTTCATTGTGCACATGCACCGGAAAGCGATCAGGGTGGTCGTACCACCTTTGTTAATACCCG
TCGTGTTGTTGCAAATGCAACCCAGCAGCAGCTGGAACAGTGGAAAAACATTAGCATTACCTAC
CGCATCAACAAAGTGACCCATTATGGTGGTGAAGTTCATAGTCCGCTGGTTGAAGAACATCCGG
ATCGTAATGGTTTTGTGATTCGTTATAATGAACCGGCAGTGGATGGTGAAAAATTCCTGAATAA
ACACGCCATCGAGTACCATAACATTAATCCGGATCAGGTTGCAGAATTTCAGCAGGATTTTATC
AACATCCTGTATGATAAACGCCATCTGTATGCACATGCCTGGAAAAAAAGTGATCTGGTGATTG
TGGATAACTTTAGCCTGCTGCATGGTCGTGAAGGTTTTACCAGCAAAAGCGAACGTCATCTGCA
GCGTATTCATATTCAGAGCAATCCGGCATTTAACAATCAGGCACTGCGTAGCTAAGAATTCGAG
CTCCGTCGACAAGCTTGCGGCCGCACTCGAGC

**Over-expression and Purification of *P*.IsnB.**

The plasmid encoding p*isnB* gene described above was transformed into *E. coli* BL21 (DE3) cells (New England Biolabs, MA). A single colony was picked and incubated with 10 mL LB at 37 °C for ~ 16 hours. The cells were used as starting culture for large scale *P*.IsnB expression with a volumetric ratio of 1:100 of starting culture to growth media. After inoculation, LB growth medium with 50 ug/mL kanamycin at 37 °C with shaking at 220 rpm. Upon reaching an $OD_{600}$ of ~ 0.6, IPTG with final concentration of 0.3 mM was added to the culture, and incubation with shaking was allowed to continue at 18 °C for 12 hours before harvesting by centrifugation at 4 °C. The cell pellets were stored at -80 °C. The cells were thawed and suspended in an ice-chilled buffer with 100 mM Tris (pH 7.5), and 100 mM NaCl, and lysed by sonication. The resulting lysate was subjected to centrifugation for 20 minutes at 18,000 g at 4 °C, and the supernatant was loaded onto a Ni-NTA agarose column. The column was washed with 6 volumes of buffer containing 100 mM Tris (pH 7.5), and 100 mM NaCl. Subsequently, the desired protein was eluted using buffer containing 100 mM Tris (pH 7.5), and 100 mM NaCl, and 200 mM imidazole. Fractions containing *P*.IsnB protein were observed by SDS-PAGE, and concentrated to a volume of approximately 5 mL using Millipore® centrifugal filter. The protein solution was then dialyzed against 2 L of buffer with 10 mM EDTA, 100 mM Tris (pH 7.5) and 100 mM NaCl, and then twice against 2 L of buffer (100 mM Tris (pH 7.5) and 100 mM NaCl). It was then placed in a sealed flask on ice connected to a Schlenk line to remove $O_2$ by exchanging into nitrogen atmosphere. The degassed protein was transferred into a glove box, aliquoted to cryovials, and frozen in liquid nitrogen for assay. Protein concentration was determined by UV absorption at 280 nm using a calculated molar absorptivity of 43,890 $M^{-1}cm^{-1}$ (http://ca.expasy.org). The purity of protein was shown by SDS–PAGE gel (12% Coomassie-stained) in Fig. S23.

**Preparation of NO treated *P*.IsnB solution.**

Diethylamine (DEA) NONOate (Cayman Chemical) was used as the NO source, which releases 1.5 moles of NO gas from per mole of parent compound with a half-life of 16 mins at 22-25 $^{o}$C at pH7.4. To prepare NO treated *P*.IsnB solutions, apo *P*.IsnB was first incubated anaerobically with Fe(II) and 2OG to form the *P*.IsnB•Fe(II)•2OG tertiary complex, or with the further addition of the substrates (**1**, D-**1** or **5**) to form the *P*.IsnB•Fe(II)•2OG•substrate quaternary complex. DEA NONOate powder was then anaerobically dissolved in buffer containing 100mM Tris-HCl (pH 7.5) and 100 mM NaCl to make 100 mM NONOate stock solution. Then an

appropriate amount of such a stock solution, which will generate ideally 5 mM (final concentration) NO gas, was added into the *P*.IsnB tertiary complex and the *P*.IsnB quaternary complex. The solutions were further incubated anaerobically for 30 mins at room temperature before transferred into EPR tubes and frozen. The final sample concentrations are listed in the figure caption of Figure S29.

**Stopped-flow absorption spectroscopy characterization of *P*.IsnB.**

Stopped-flow absorption spectroscopy (SF-Abs) experiments were performed on an Applied Photophysics SX20 stopped-flow spectrometer operating in an MBraun UNilab glove box filled with nitrogen gas and maintained at < 0.5ppm $O_2$ level. Solutions were either degassed on a Schlenk line before transferring into the glove box, or prepared in an inert atmosphere box. An $O_2$ saturated buffer solution (~1.8 mM $O_2$ in a 100mM Tris-HCl (pH 7.5), 100 mM NaCl buffer solution prepared at ~4 $^0$C) was rapidly mixed at 5 $^o$C with an equal volume of an oxygen-free solution containing *P*.IsnB (0.6 mM), Fe(II) (0.54 mM), 2OG (5.4 mM), and substrate (1.35 mM) to initiate the reaction. Absorbance scans from 300 to 700 nm were collected with a photodiode-array detector at 5 $^o$C. The resulting data were processed using KaleidaGraph software. The kinetic simulations were performed by using KinTek Explorer ver. 6.13.[1]

**Freeze-quench Mössbauer experiment**

Freeze-quench experiments were performed using a KinTek quench-flow instrument. Analogous to the stopped-flow experiments, an oxygen-saturated buffer solution (~1.8 mM $O_2$ in a 100 mM Tris-HCl (pH 7.5), 100 mM NaCl buffer solution prepared at ~ 4 $^o$C) was rapidly mixed with an equal volume of an oxygen-free solution containing *P*.IsnB (1.8 mM), $^{57}$Fe(II) (1.62 mM), 2OG (16.2 mM), and substrate (**1**, or D-**1**, 4.0 mM) to initiate the reaction at 6 $^o$C. The resulting reaction was terminated by injection of the solution into liquid ethane maintained at 90 K at various time points. The resulting samples were first pumped to remove liquid ethane. Then the dry frozen solution powder was packed into in-house designed freeze quench Mössbauer sample cups at 77 K to generate Mössbauer samples. The reaction time of a freeze-quenched sample is the sum of the aging time and the quench time. The aging time was the transit time for the reaction mixture through the aging hose. The quench time corresponded to the time required after injection into the cryosolvent for the reaction mixture to be cooled sufficiently to prevent further reaction and was estimated to be ~ 5 ms.

**Mössbauer Analysis**

Mössbauer spectra were recorded with home built spectrometers using Janis Research Super-Varitemp dewars, which allowed studies in the temperature range from 1.5 to 200 K, and applied magnetic fields up to 8.0 T. Mössbauer spectral simulations were performed using the WMOSS software package (SEE Co., Edina, MN). Isomer shifts are quoted relative to Fe metal at 298 K. All Mössbauer figures were prepared using SpinCount software.[2]

**X-Band CW EPR experiment**

X-band EPR spectra were measured on a Bruker Elexsys E-500 spectrometer equipped with an Oxford ESP-910 cryostat. The instrument conditions for the measurements were microwave frequency, 9.64 GHz, microwave power, 0.2 mW; modulation frequency, 100 kHz; modulation amplitude, 10G. The spectral simulations were performed by using the SpinCount software.[2]

**HYSCORE experiment**

Q-band (33.83 GHz) pulsed EPR spectra were recorded using a custom-built ELEXSYS E580 spectrometer equipped with SuperQ-FT bridge, SuperQ-FT solid state 10 W amplifier and EN5107D2 resonator. All spectra were measured at T=3.1 K maintained inside ER 4118CF helium flow cryostat by ER 4112HV-1017 temperature controller (all from BrukerBiospin, Billerica, MA). Duration of 90° and 180° microwave pulses was 8 ns and 14 ns respectively.

Hyperfine sublevel correlation (HYSCORE) spectrum was acquired using a four-pulse sequence with 16-step phase cycling scheme.[3] Due to fast electron spin relaxation rates, the interval between the first and the second pulses was set as short as 140 ns. For shorter time separations, ring-down effects started to be significant increasing the noise of the detected signals. Delays between the second and the third pulses in the first dimension and between the third and the fourth pulses in the second dimension were incremented by 8 ns steps from their initial values of 24 ns and 32 ns, respectively. Pulse delays were defined as time delays between the starting points of the pulses. The difference between the initial delays was set to 6 ns to improve symmetry of the measured HYSCORE spectra with respect to two dimensions by taking into account the difference in pulse durations. Time domain HYSCORE spectra were recorded as [500×500] matrix. A third power polynomial baseline correction was applied, followed by a Hamming window apodization. Time domain data were zero filled to yield [2048×2048] matrix,

Fourier transformed, and plotted using a "contour" function of Matlab R2012a (MathWorks, Natick, MA).

Simulations of $^2$H-HYSCORE spectra were carried out using EasySpin-5.2.20[4] based on treating the observed lower Kramer's doublet $S = \frac{3}{2}, m_S = +\frac{1}{2} \leftrightarrow -\frac{1}{2}$ transitions as an effective $S = \frac{1}{2}$ system. In such HYSCORE spectra the electron-nuclear hyperfine interaction, *A*, is detected as an effective hyperfine interaction $A_{eff} \approx 2A$ while the quadrupole parameters remain unchanged.[5] No orientational selectivity has been assumed in the simulations.

**LC-MS study of IsnB reaction**

High performance liquid chromatography (HPLC) with detection by UV and mass spectrometry (MS) were conducted on an Agilent Technologies (Santa Clara, CA) 1200 system coupled to an Agilent Technologies 1260 diode array detector and an Agilent Technologies 6120 quadrupole mass spectrometer. The associated Agilent MassHunter and OpenLAB software package were used for data collection and analysis. Assay mixtures were separated on an Agilent ZORBAX Extended-C18 column (4.6 x 50 mm, 1.8 μm particle size) with isocratic system of 50% of solvent A (20mM aqueous ammonium formate, pH 6.8) and 50% solvent B (acetonitrile) for UV detection and a gradient of 95–45 % B was applied from 2 to 4 min, and then a gradient from 45–98 % B was applied from 9 to 11 min. The column was allowed to re-equilibrate for 2 min under initial conditions before subsequent sample injections. for MS detection. Detection was performed using electrospray ionization in negative mode ($ESI^-$) and absorbance at 266 nm.

Reactions associated with **Figure 4a-b** and **Figure S24a** were performed as described below. An anaerobic solution of *P*.IsnB•$Fe^{II}$•2OG•substrate (**1**, **3**, **4**, or **5**) was mixed with equal volume of an oxygenated buffer on ice with the final concentrations of 0.1 mM $Fe^{II}$, 0.12 mM *P*.IsnB, 0.30 mM of substrate, and 0.30 mM of 2OG in a total volume of 400 uL. After 5 minutes, the reaction was halted by adding 200 uL of acetonitrile. For the reaction associated **Figure 4c**, the reaction mixture containing *P*.IsnB•$Fe^{II}$•**9** with final concentration of 0.1 mM $Fe^{II}$, 0.11 mM *P*.IsnB, and 0.30 mM of **9**, was kept on ice in the anaerobic chamber and the reaction was quenched at 20 mins. We reason that if *P*.IsnB can catalyze conversion of **9** to **6**, it is likely to proceed through $CO_2$ elimination and followed by OH (most likely at its protonated from) group departure. Hence, formation of the presumptive Fe(IV)=O species is not required and the experiment was

carried under anaerobic condition. Prior to LC-UV and LV-MS analysis, all reaction samples were centrifuged (12,000 g) to precipitate protein.

To elucidate the possible binding of **9** with protein, *P*.IsnB was incubated with **9** on ice for 5 min anaerobically. Native substrate (**1**) and 2OG were then added to the reaction mixture and exposed reaction to air for 5 mins with inal concentrations of 0.1 mM $Fe^{II}$, 0.12 mM *P*.IsnB, 0.30 mM of **1**, 0.50 mM of **9** and 0.50 mM of 2OG in a total volume of 400 uL. Subsequently, the reaction mixture was quenched and analyzed as described previously (**Figure S24b**). The control experiment was conducted by reconstituted *P*.IsnB anaerobically for 4 mins and followed by addition of **1** and 2OG. To probe the origin of oxygen of hydroxylated product when analog (**3**) was used, the reaction was conducted in ~ 87% $^{18}O$ enriched $^{18}OH_2$ buffer with the procedure described previously (**Figure S24c**). $^{18}OH_2$ buffer was prepared by mixing concentrated Tris-HCl (2.0 M) with $^{18}O$-water (purchased from Cambridge Isotope Laboratory) in a volumetric ratio of 1 to 19. The protein was prepared using $^{16}OH_2$ buffer. After adding protein, 2OG, and the substrate, the $^{18}O$ content in the reaction mixture is ~ 87%.

**Comments on SF-Abs kinetic analysis**

Kinetic analyses were carried out on the 440 nm and 512 nm optical traces obtained by the SF-Abs measurements on the *P*.IsnB reactions using compounds **1**, D-**1**, **3**, **4**, and **5**. The 512 nm optical traces represent mainly the *P*.IsnB•Fe(II)•2OG•substrate quaternary complex and the *P*.IsnB•Fe(II)•2OG tertiary complex (Fig. S25). The quaternary complex showed different Fe-2OG MLCT band than that of the tertiary complex. Specifically, the Fe-2OG MLCT band from the quaternary complex is peaked at 512 nm with distinct absorption shoulders at 465 and 570 nm. In contrast, only a broad absorption feature centered at ~ 500 nm is observed for the tertiary complex. To characterize the kinetics of the ferryl intermediate, we used the 440 nm optical feature instead of the 320 nm optical feature that was used routinely for monitoring the ferryl intermediate kinetics in TauD and SyrB2.[6, 7] For *P*.IsnB, the absorption change below 350 nm cannot be unambiguously assigned and it may be partially resulted from the products generated in the reaction (Fig. S26). This complication renders the 320 nm feature ineffective for reporting the kinetics of such an intermediate. Thus, we used 440nm feature throughout this study as the characteristic wavelength for the Fe(IV)=O species. It is supported by the Mössbauer results

presented in this study. A three-step model kinetic model can reproduce the time dependent changes of the 440 nm and 512 nm optical features for all the reactions studied by SF-Abs in this work, which can be described as *P*.IsnB•Fe(II)•2OG•substrate quaternary complex + $O_2$ → Fe(IV)=O → *P*.IsnB-product complex → *P*.IsnB•Fe(II)•2OG tertiary complex. The suitability of this model to describe the kinetic behavior of *P*.IsnB reactions was derived from simultaneous simulations of *P*.IsnB reactions with **1** and D-**1** (Fig. S27). In the reaction of *P*.IsnB with **1**, the 440 nm and the 512 nm traces were mainly the result of the *P*.IsnB•Fe(II)•2OG•**1** decay (up to 0.07 s) and the reformation of the *P*.IsnB•Fe(II)•2OG tertiary complex (after ~ 0.1 s). No observable accumulation of the ferryl intermediate was detected, which is consistent with the FQ Mössbauer results (See Fig. S31). The evidence that the reformed species is the tertiary complex instead of the quaternary complex came from the comparison of the optical features of the Fe(II)-2OG MLCT band before and after the reaction (Fig. S28). Figure S28 clearly shows that the reformed species exhibits MLCT band feature which is different from the quaternary complex (please compare to Fig. S25). When D-**1** was used, a clear accumulation of the ferryl intermediate was observed in the 440 nm trace. Compared to **1**, the apparent slowdown of the decay kinetics of the 512 nm trace (up to 0.3 s) is consistent with that the observation that the ferryl intermediate contributes to the absorption feature at ~512 nm.[6, 8] Therefore, the time dependent absorption change at 512 nm up to ~ 0.3 s in the reaction when D-**1** was used reflects mainly the combination of the decay of the quaternary complex and the kinetics of the ferryl intermediate. By simultaneously simulating the 440 nm and the 512 nm traces in both reactions (**1** and D-**1**), a set of rate constants were obtained, with $k_1$ ~ 65 $mM^{-1}s^{-1}$ (the decay rate constant of the quaternary complex), $k_2$ > 300 $s^{-1}$ for **1** and = 2.5±0.5 $s^{-1}$ for D-**1** (the decay rate constant of the ferryl intermediate), and $k_3$ = 3±1 $s^{-1}$ (the apparent reformation rate constant of the *P*.IsnB tertiary complex). This kinetic model was also used to simulate the time-dependent absorption changes of the 440 nm and the 512 nm features observed for the reactions when **3**, **4**, or **5** analogs were used. The simulations suggested that all three substrate analogs have similar but slightly smaller decay rate constants of the quaternary complex ($k_1$) than the value determined in the reaction with **1**. Decay constant ($k_1$) ranged from 40 – 50 $mM^{-1}$ $s^{-1}$ for these substrate analogs were observed. In addition, the accumulation of the ferryl intermediate was observed when substrate analogs were used (Fig. S27) and the decay rate constants ($k_2$) were determined to be 19±2 $s^{-1}$ for **3**, 10±2 $s^{-1}$ for **4**, and 3±1 $s^{-1}$ for **5**, respectively.

**Comments on Mössbauer analysis**

Freeze-quench (FQ) coupled Mössbauer spectroscopy was used to validate the kinetic analyses derived from the SF-Abs experiments. Three quadrupole doublets were observed in the sample containing the anaerobic *P*.IsnB•Fe(II)•2OG•**1** (or D-**1**) complex (Fig. S31). The major doublet, representing 67% of the total iron in the sample, has an isomer shift (δ) of 1.18 mm/s and quadrupole splittings ($|\Delta E_Q|$) of 2.76 mm/s, which are typical parameters from a high-spin ($S$ = 2) ferrous species. A second doublet, representing 20% of the iron in the sample, has δ = 0.27 mm/s and $|\Delta E_Q|$ = 0.47 mm/s, which most likely originates from a low spin ($S$ = 0) isonitrile-Fe(II) complex. A similar iron species has also been observed in the *trans*-indoyl vinyl isonitrile synthase, IsnB.[9] This isonitrile-Fe(II) complex is inactive towards $O_2$, therefore, does not involved in *P*.IsnB reaction (see Table S1). A third quadrupole doublet, representing only ~ 10% of the iron (δ = 1.26 mm/s and $|\Delta E_Q|$ = 3.37 mm/s), is also inactive towards $O_2$ (see Table S1). This minor species, again typical of a high-spin ferrous species, most likely belongs to a portion of inactive enzyme, which has also been observed in the Mössbauer analysis on AsqJ reactions.[10] After the rapid mixing of the *P*.IsnB quaternary complex with $O_2$ saturated buffer, a new quadrupole doublet, representing a new high-spin ferrous species, developed at 0.02 s (the earliest time point used in this study) to 27 % with δ = 1.28 mm/s and $|\Delta E_Q|$ = 2.84 mm/s when **1** was used. Simultaneously, the doublet representing the *P*.IsnB quaternary complex decreased by 28 % (Fig. S31, Table S2). Thus the formation of the new doublet was in expense of the quaternary complex. This new doublet is clearly distinct from the doublet representing the *P*.IsnB quaternary complex, which is evidenced by the position difference of the high-energy absorption line of these two quadrupole doublets (Fig. S31). This new doublet was further increased to 32 % at 0.07 s, and did not change up to 5 s after the mixing of $O_2$ (Fig. S31). Based on the kinetic analysis of the SF-Abs data, two ferrous species should be observed after the mixing of $O_2$ in *P*.IsnB reaction, which are the iron centers from the *P*.IsnB-product complex and the *P*.IsnB•Fe(II)•2OG tertiary complex. Yet, only one ferrous species was observed in Mössbauer after the *P*.IsnB quaternary complex reacted with $O_2$. One possible scenario is that the iron centers in both complexes produce indistinguishable Mössbauer quadrupole doublets, which lead to the observation of only one new ferrous doublet. In addition, the ferryl intermediate was not observed in the FQ Mössbauer samples when **1** was used. In contrast, a

quadrupole doublet with δ= 0.29 mm/s, $|\Delta E_Q|$ = 1.06 mm/s was observed at 0.02 s in the reaction when D-**1** was used. These Mössbauer parameters confirmed that this doublet is originated from the ferryl intermediate (Please refer to Table S1 of the cited reference).[10] At the same time, the accumulation of the enzyme-product/*P*.IsnB•Fe(II)•2OG complex was only at 10%. At 0.07 s, the ferryl intermediate was accumulated at a similar level (17%) as that at 0.02 s. At 0.25 s, the ferryl intermediate decreased to 8%, and further decreased to an undetectable level at 5 s. The maximum accumulation of the ferryl intermediate (~ 20% of the total iron in the sample, or ~ 30% of the total *P*.IsnB quaternary complex, Table S2) seems lower than the expected level based on the kinetic model we used to simulate the SF-Abs data. However, we notice that even at the time point when the maximum amount of the ferryl intermediate is captured, there are still ~ 30% (relative to the iron concentration) *P*.IsnB quaternary complex remaining (Table S2), which implies that the quaternary complex only exhibits partial activity. For Fe/2OG enzymes that are prepared by the heterologous overexpression method, the partial activity of the enzyme quaternary complex is often observed. For example, for CarC, another Fe/2OG enzyme, the activity of the CarC quaternary complex was estimated to be ~ 1/3.[11] For the current case, we estimate that the activity of the *P*.IsnB quaternary complex is ~ 1/2 based on the Mössbauer analysis. Lastly, the two 5-s spectra from the two reactions (**1** and D-**1**) are identical (Fig. S31). In summary, FQ Mössbauer measurements showed that the accumulation of the ferryl intermediate can be observed only when D-**1** was used, thus confirming the kinetic analysis based on SF-Abs data, and demonstrating a large H/D KIE (> 100) for the benzylic C-H activation by the ferryl intermediate in *P*.IsnB.

**Comments on X-band CW EPR analysis**

The addition of NO to both the *P*.IsnB•Fe(II)•2OG tertiary complex and the *P*.IsnB•Fe(II)•2OG•substrate quaternary complex yielded three S = 3/2 $\{FeNO\}^7$ species with slightly different rhombicity in zero-field splitting parameters (E/D) as determined by $g \approx 4$ resonances observed in CW X-band (9.64 GHz) EPR spectra (Fig. S29). The $g \approx 4$ features originate from $m_S = \pm 1/2$ Kramer's doublet of $S = 3/2$ spin manifold. In the case of the *P*.IsnB•Fe(II)•2OG complex, CW EPR indicates the existence of three structurally distinct $\{FeNO\}^7$ species with comparable spin concentrations. However, the presence of the substrate (**1** or D-**1**) makes the axial $S = 3/2$ $\{FeNO\}^7$ species (with E/D = 0.01) as the dominate component of the spectrum with *ca*. 70% of the total $\{FeNO\}^7$ species observed (Fig. S29). These

observations suggest that the presence of the substrate may generate geometric constraints and, thus, influence the interactions between NO and the Fe(II) center of *P*.IsnB. A similar spectroscopic behavior is observed when the $CF_3$-analog is used (Figure S29), suggesting the binding configuration of this analog should be similar with that of the native substrate (**1**). It is worthy to mention that HYSCORE experiment may be used to distinguish distal and proximal type binding configuration of 2OG in Fe/2OG enzymes. Once one determines the g tensor orientation of the $\{FeNO\}^7$ complex relative to its molecular frame, $^{13}C$-labled 2OG could be used to deduce the relative orientation of 2OG.

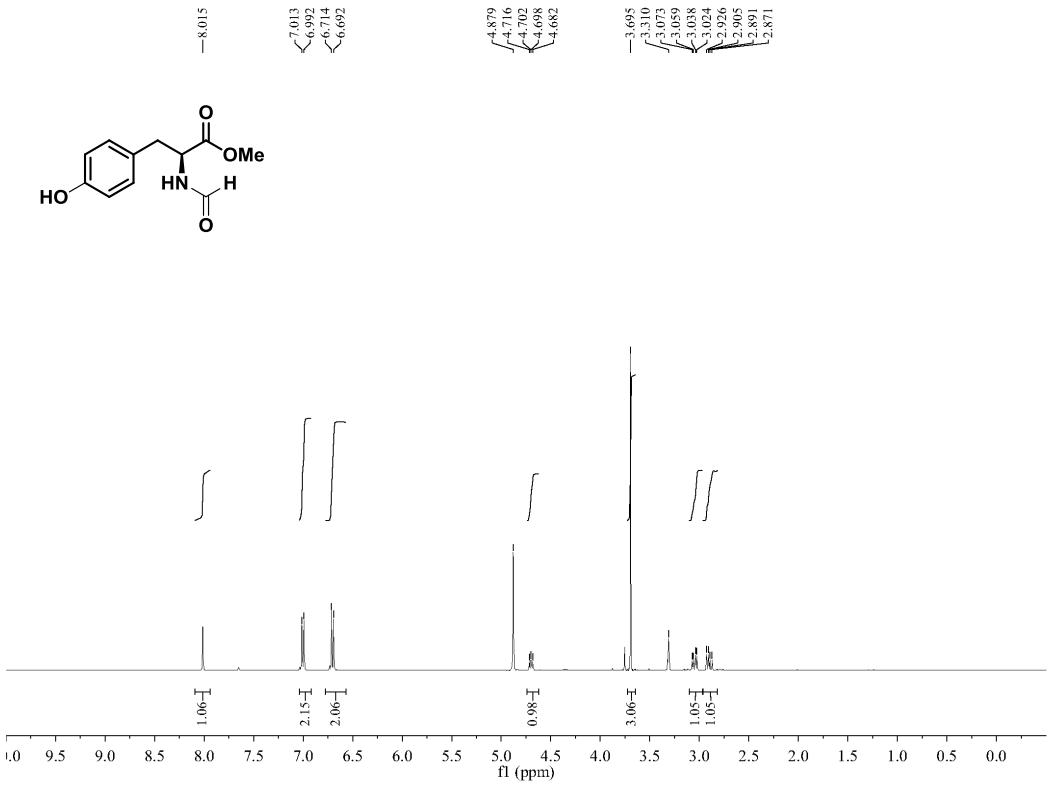


**Figure S1.** $^{1}$H NMR of methyl formyl-L-tyrosinate.

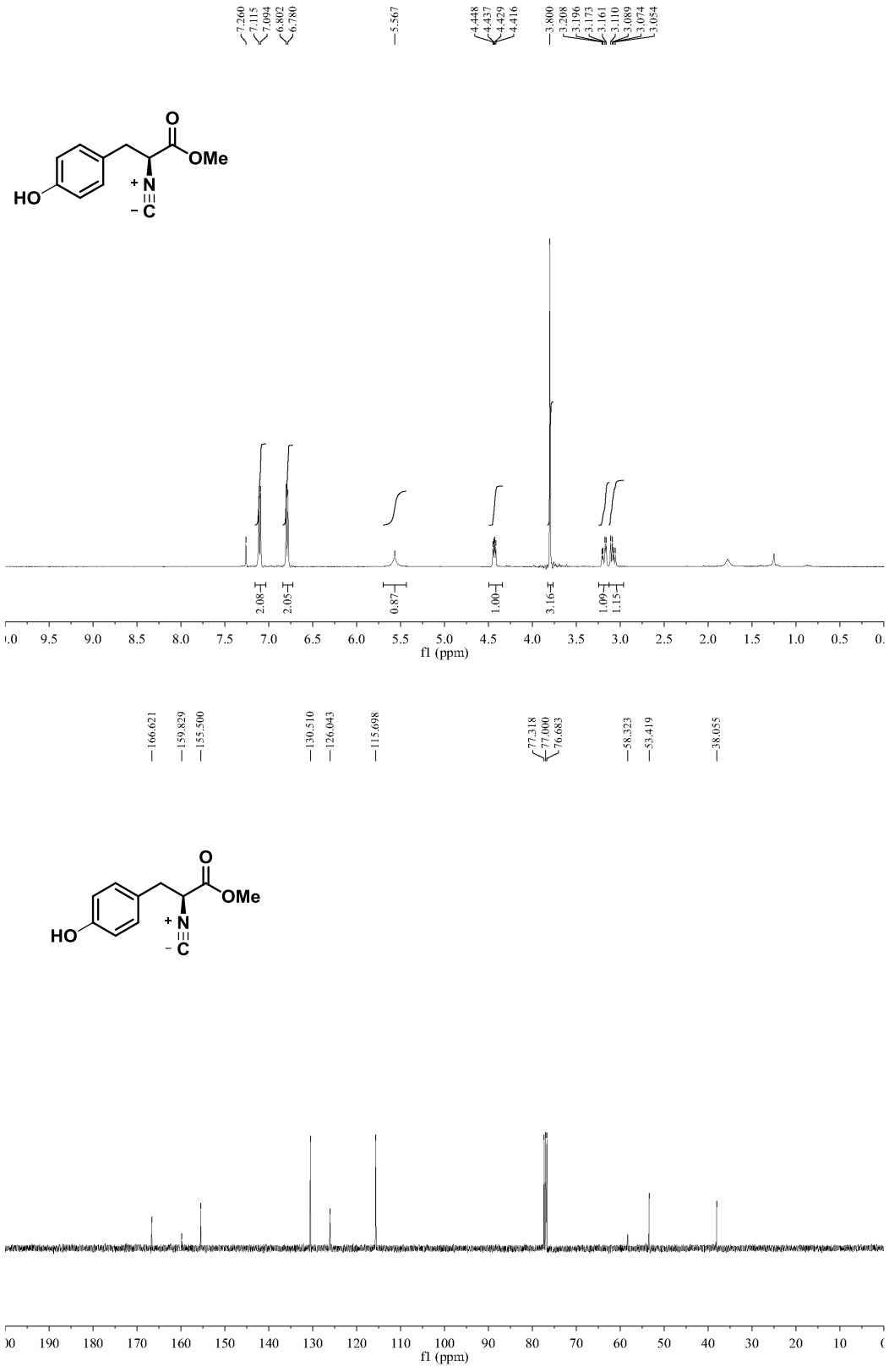


**Figure S2.** $^{1}H$ and $^{13}C$ NMR of methyl (*S*)-3-(4-hydroxyphenyl)-2-isocyanopropanoate

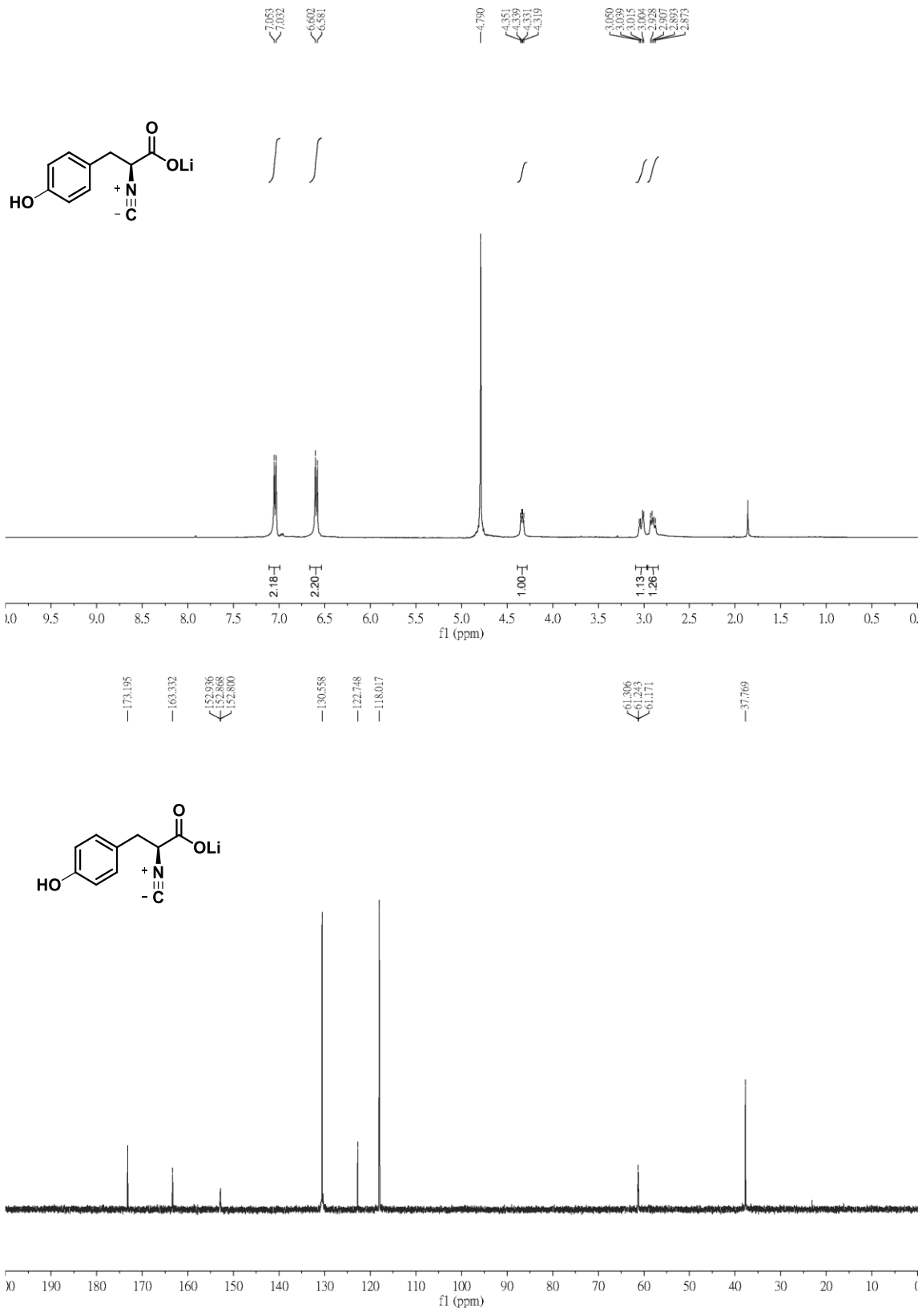


**Figure S3.** $^{1}H$ and $^{13}C$ NMR of **1**.

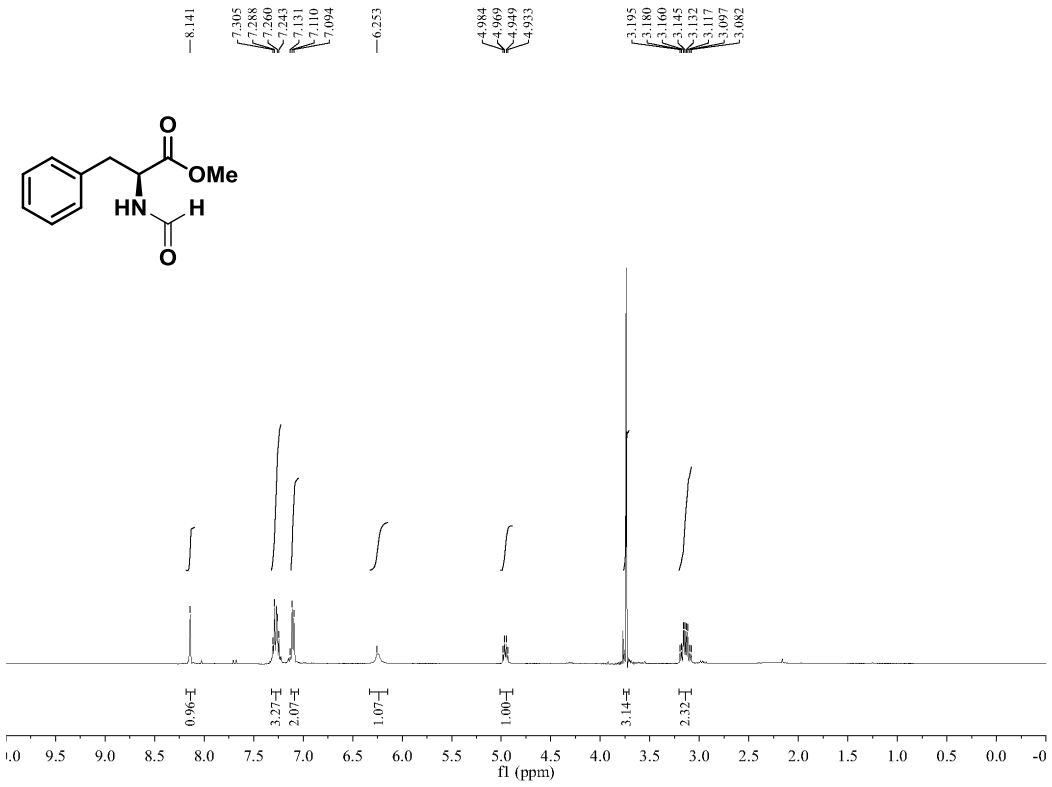


**Figure S4.** $^{1}$H NMR of methyl formyl-L-phenylalaninate.

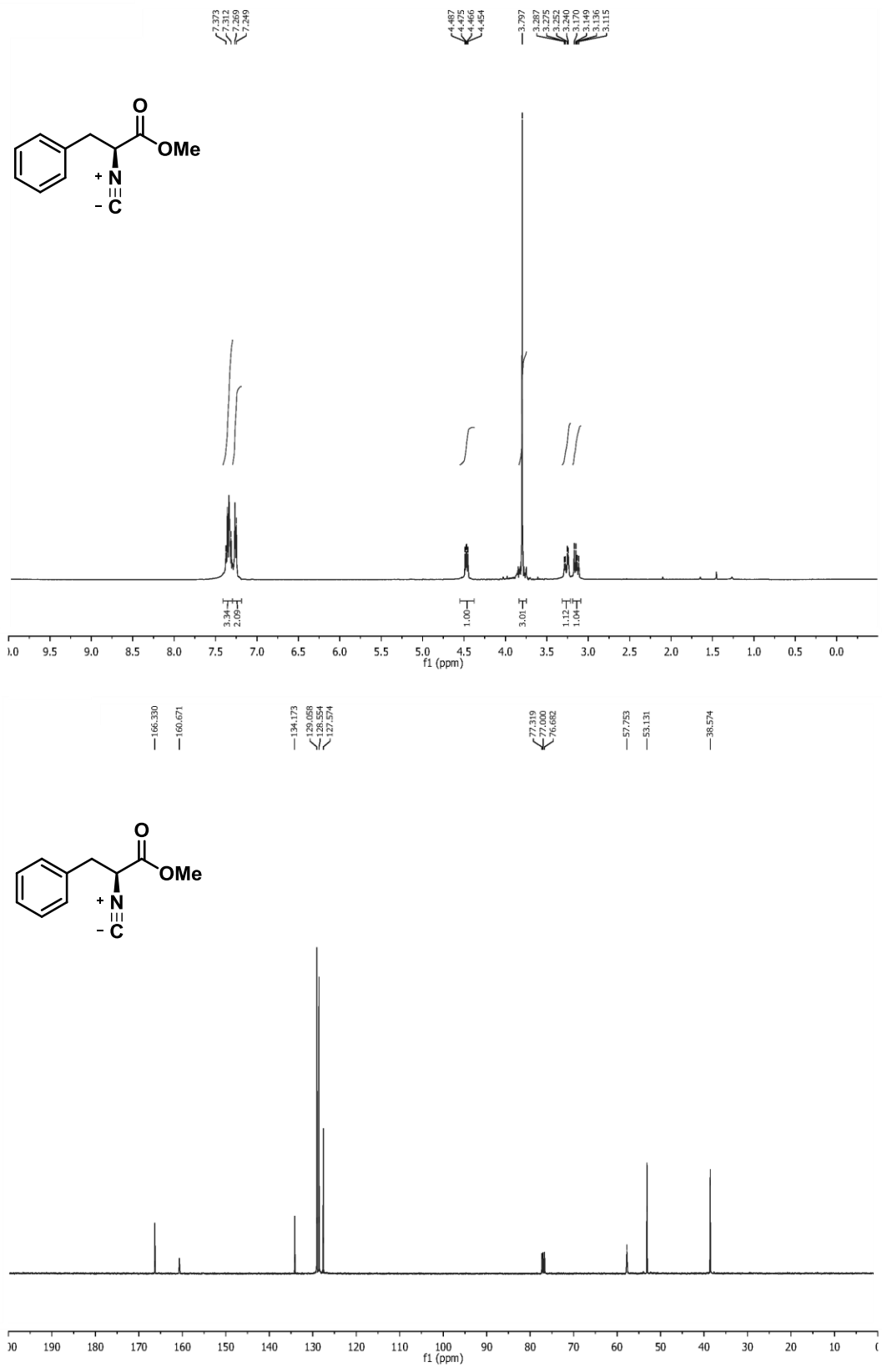


**Figure S5.** $^{1}H$ and $^{13}C$ NMR of methyl (*S*)-2-isocyano-3-phenylpropanoate.

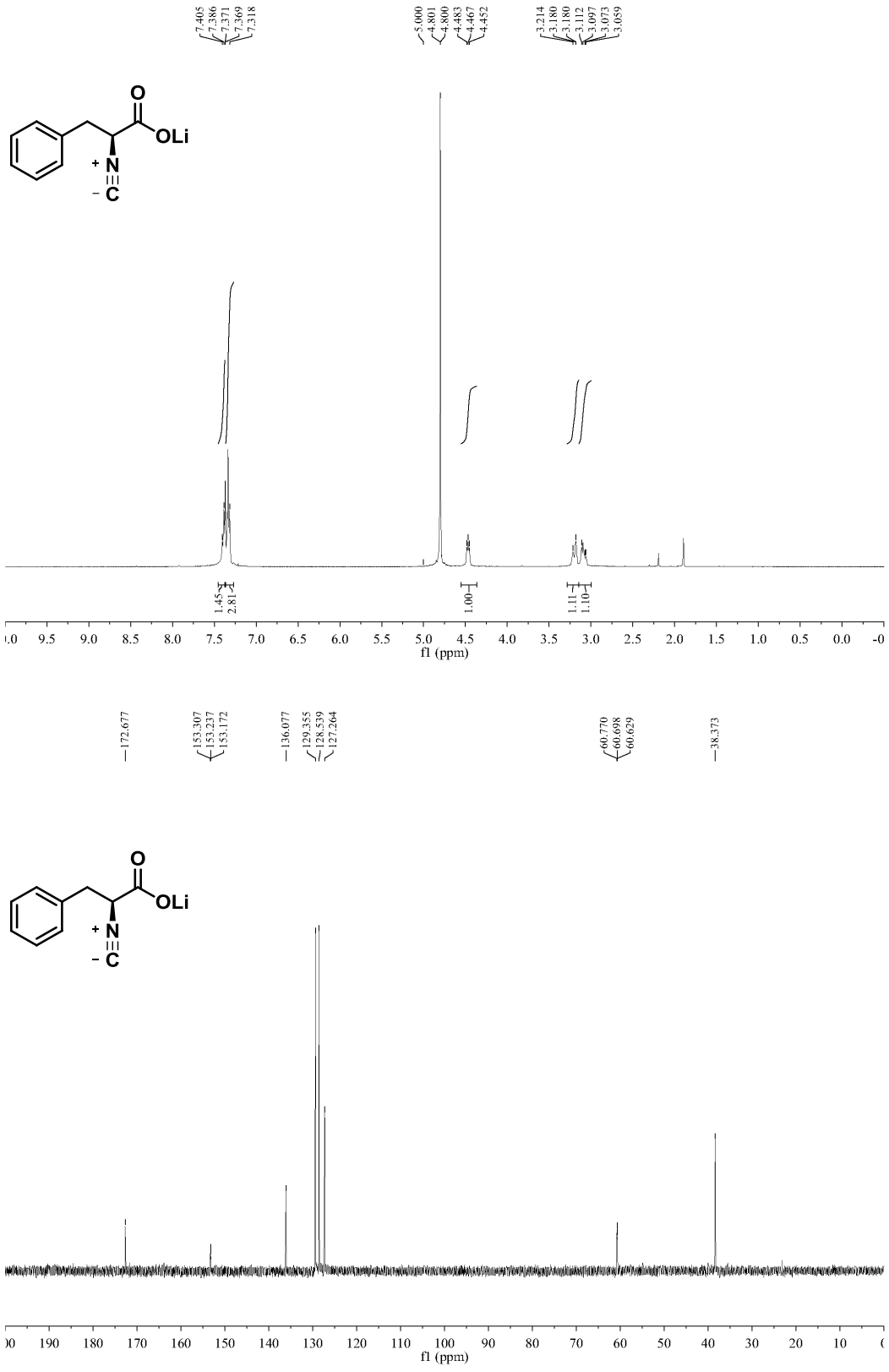


**Figure S6.** $^{1}H$ and $^{13}C$ NMR of **3**.

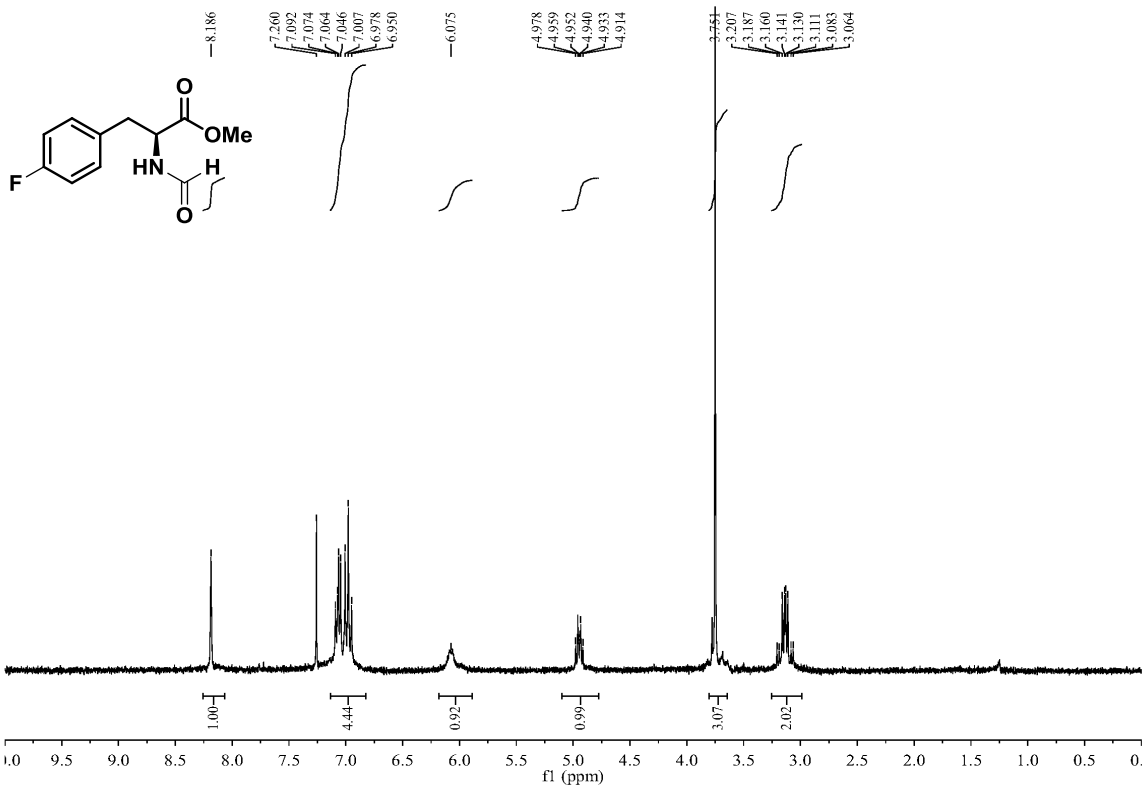


**Figure S7.** $^{1}$H NMR of methyl formyl-L-4-furoro-phenylalaninate.

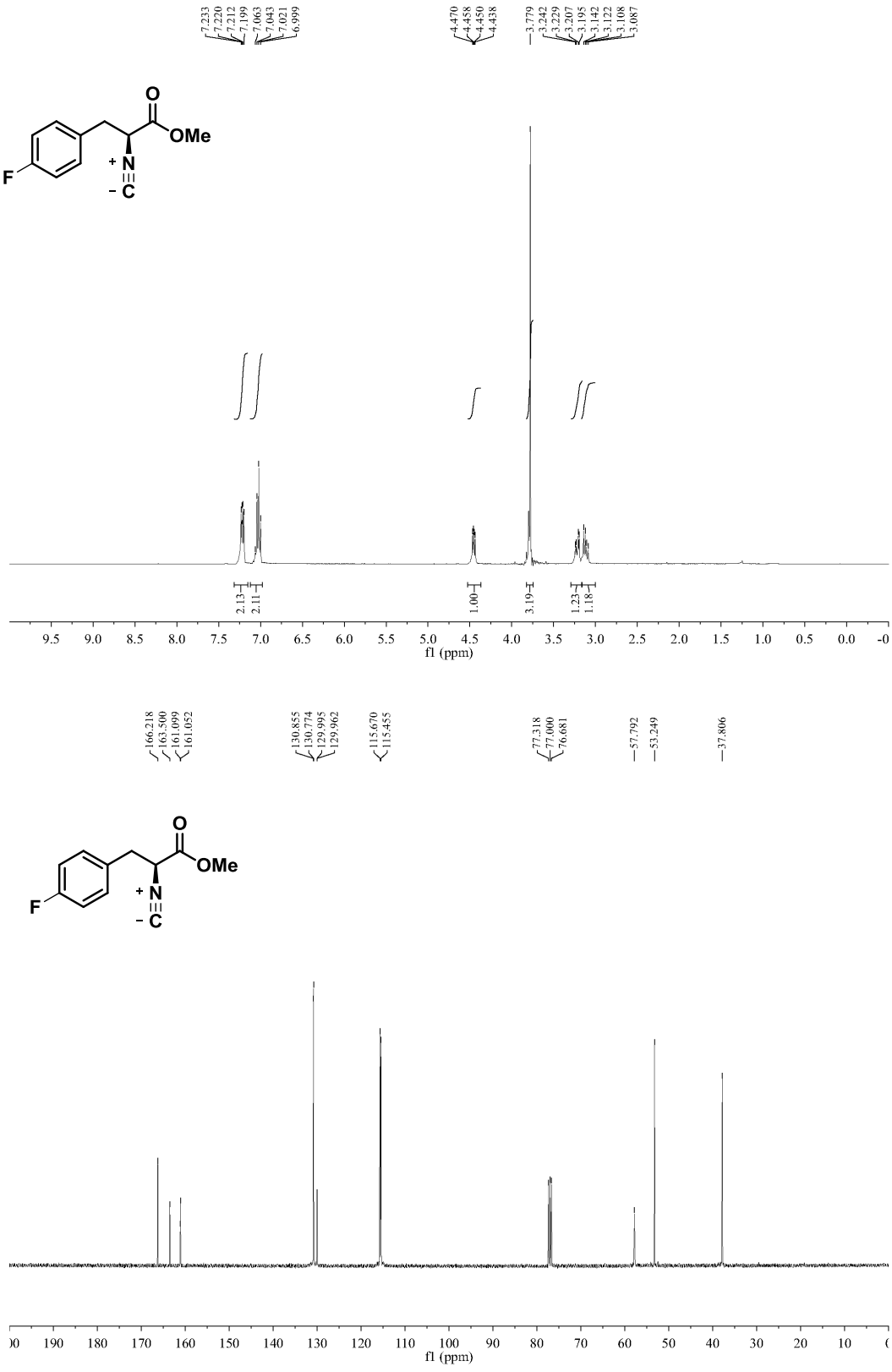


**Figure S8.** $^{1}H$ and $^{13}C$ NMR of methyl (*S*)-2-isocyano-3-(4-fluoro-phenyl)propanoate.

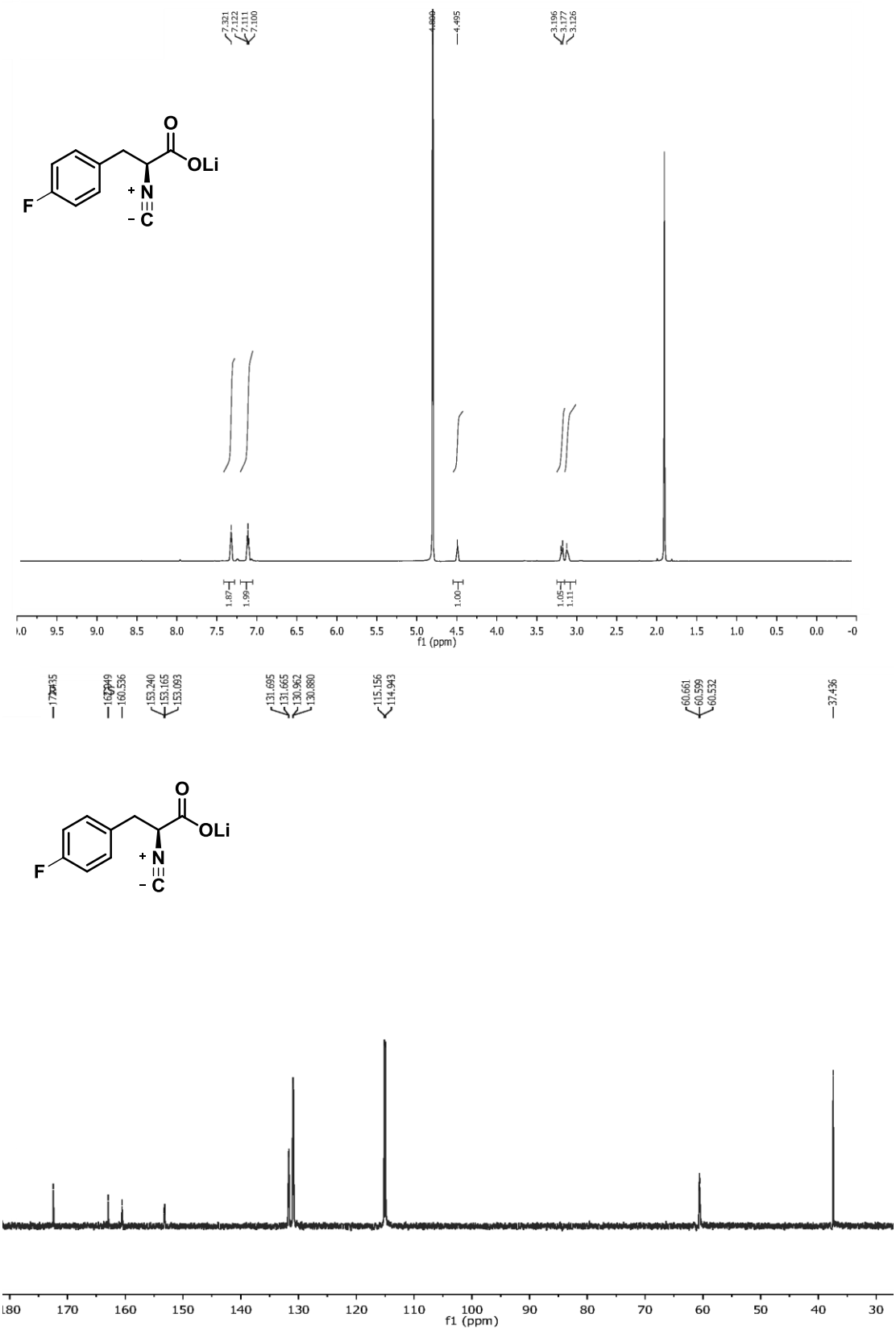


**Figure S9.** $^{1}H$ and $^{13}C$ NMR of **4**.

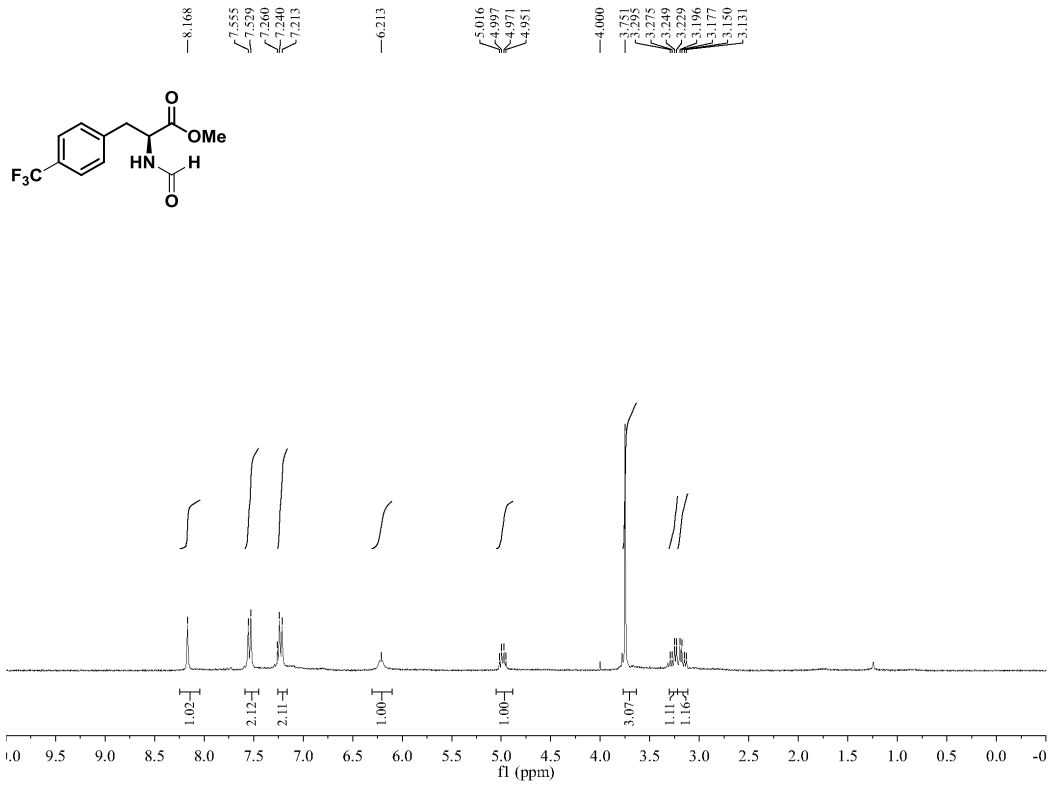


**Figure S10.** $^{1}$H NMR of methyl formyl-L-4-trifuromethyl-phenylalaninate.

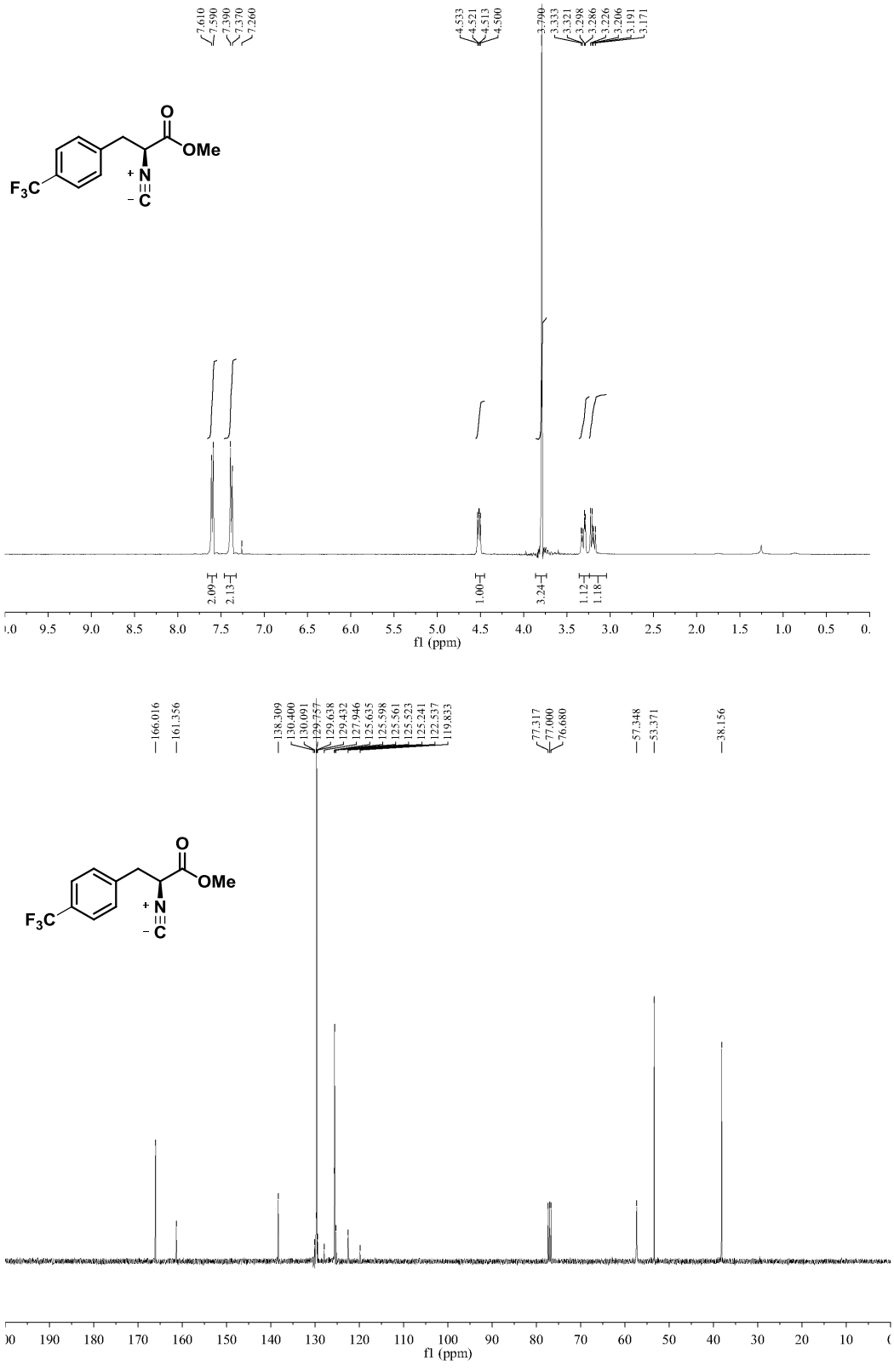


**Figure S11.** $^{1}H$ and $^{13}C$ NMR of methyl (*S*)-2-isocyano-3-(4-(trifluoromethyl) phenyl)propanoate.

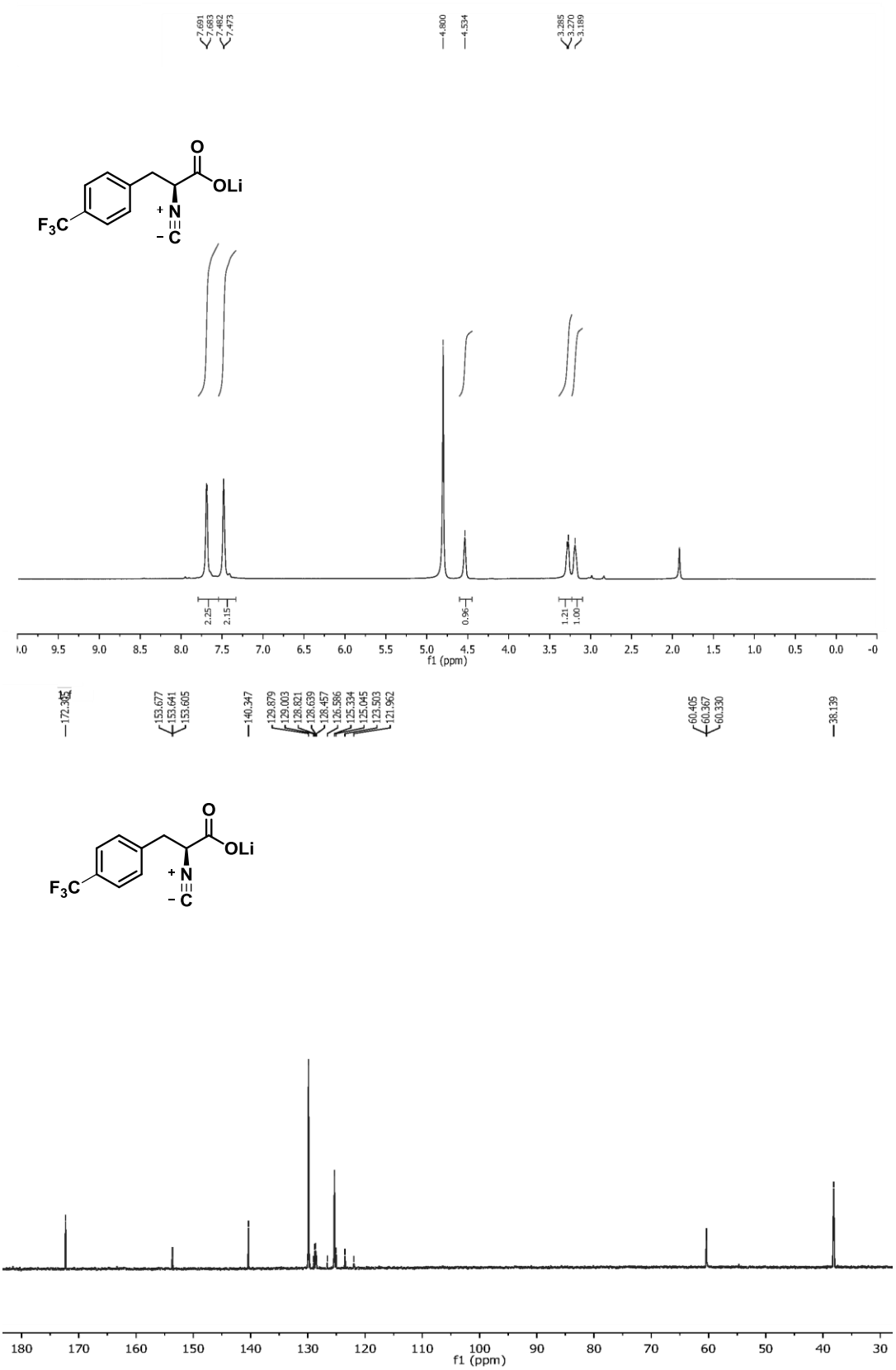


**Figure S12.** $^{1}H$ and $^{13}C$ NMR of **5**.

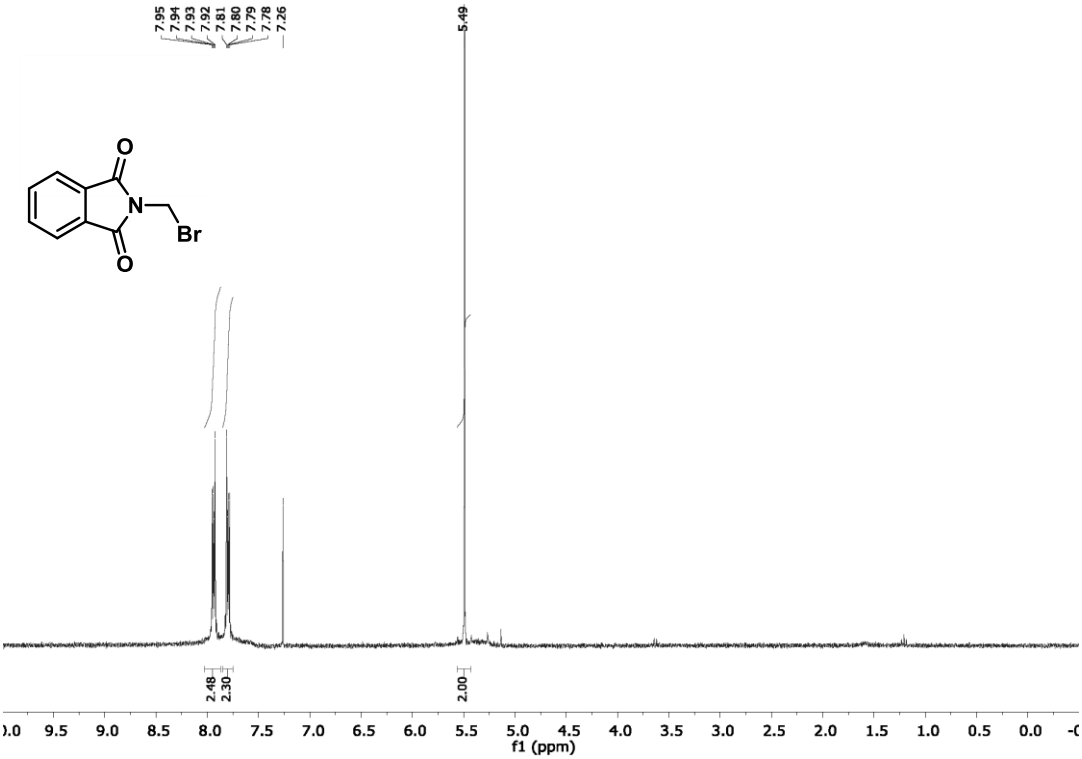


**Figure S13.** $^{1}$H NMR of *N*-bromomethylphthalimide.

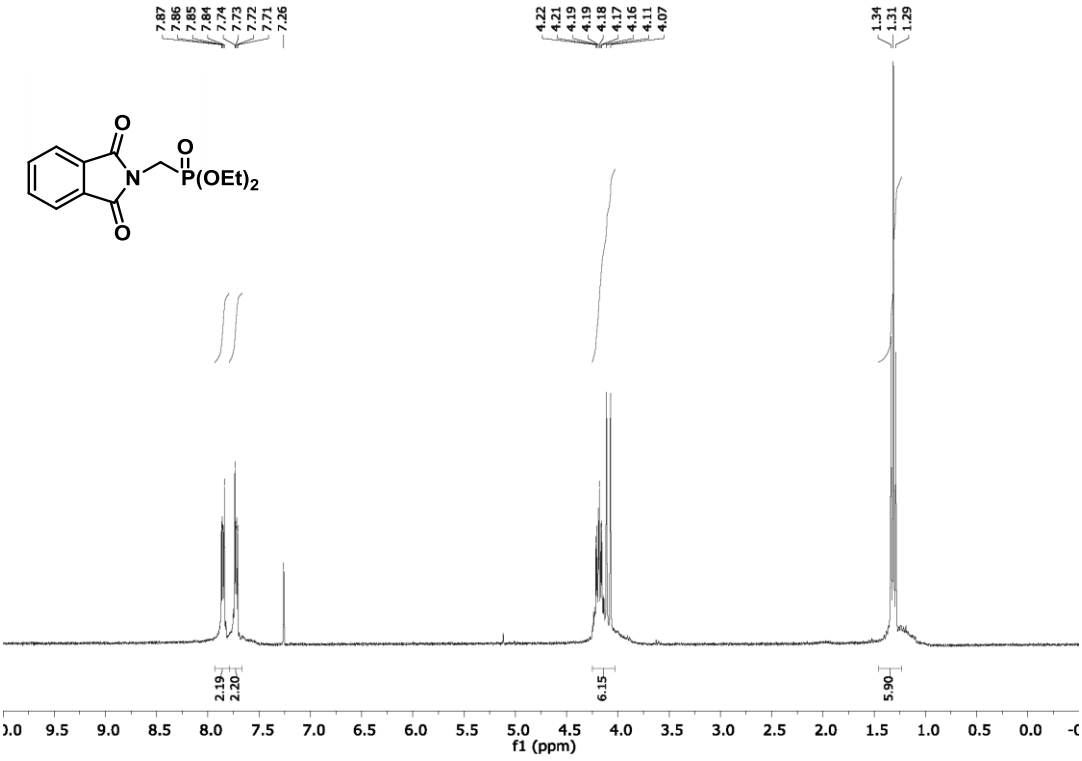


**Figure S14.** $^{1}$H NMR of diethyl phthalimidomethylphosphonate.

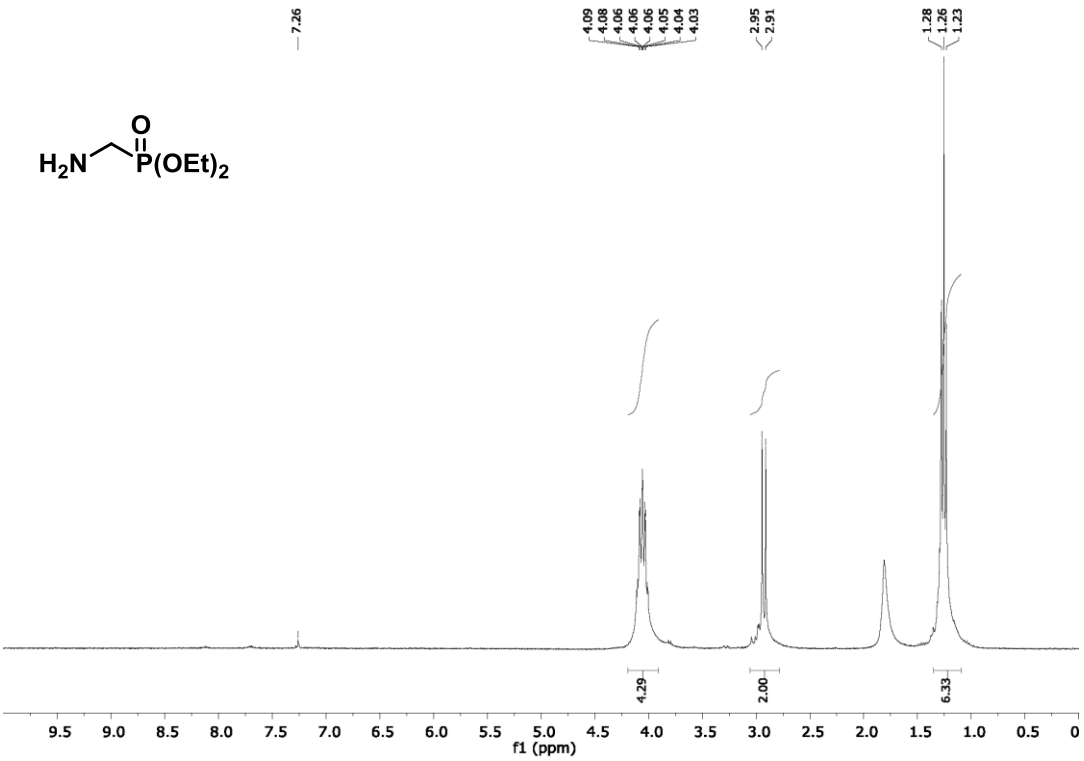


**Figure S15.** $^{1}$H NMR of diethyl(aminomethyl)phosphonate.

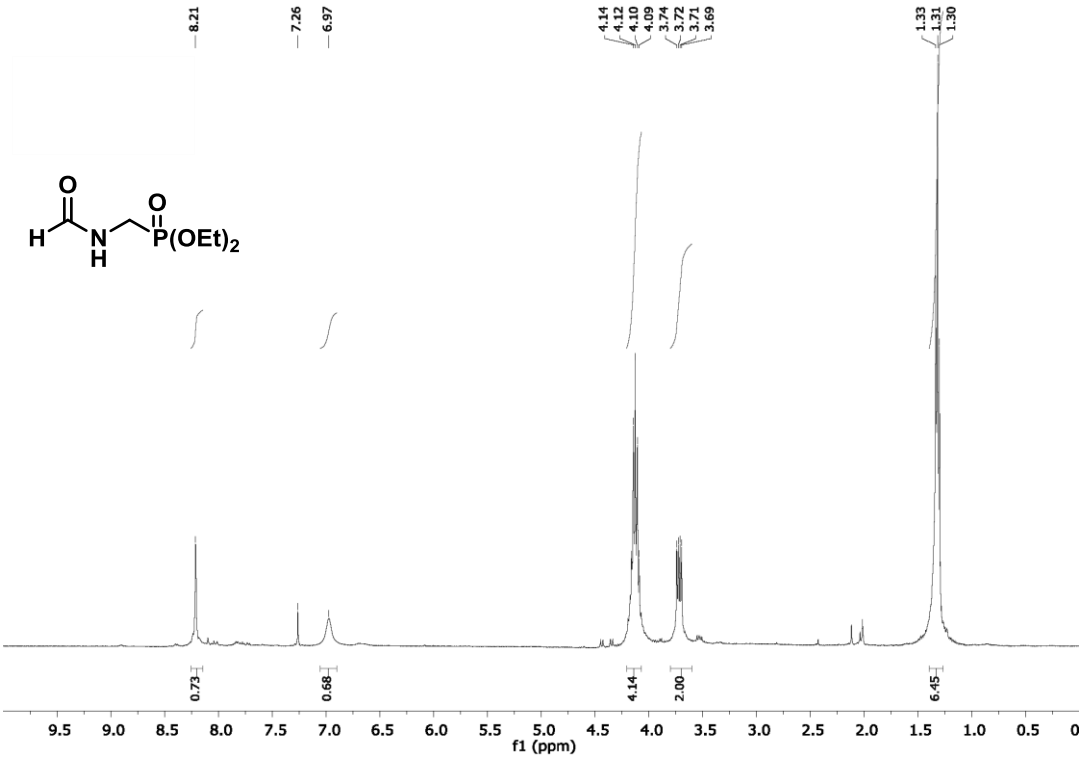


**Figure S16.** $^{1}$H NMR of diethyl (formamidomethyl)phosphonate.

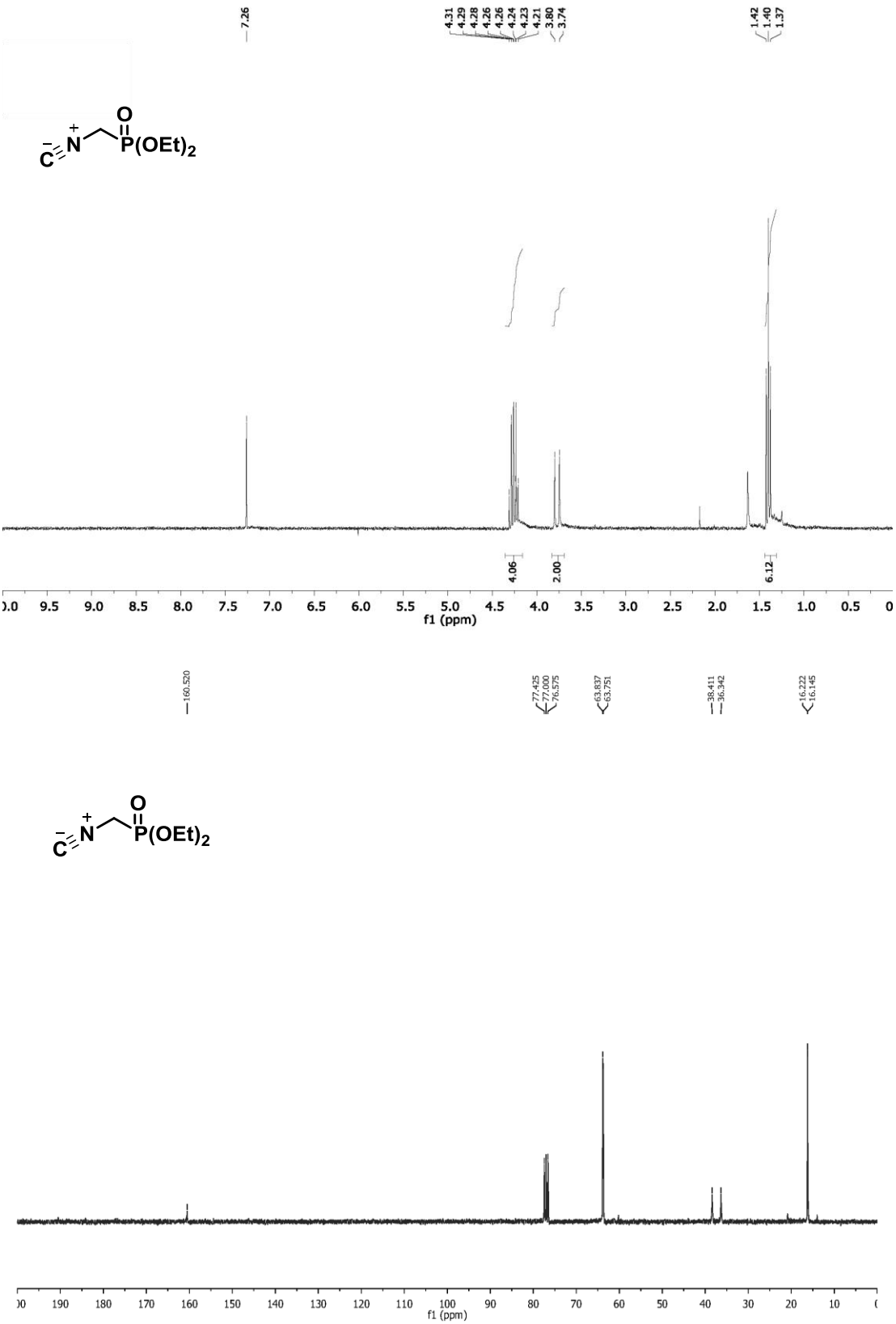


**Figure S17.** $^{1}H$ and $^{13}C$ NMR of diethyl (isocyanomethyl)phosphonate.

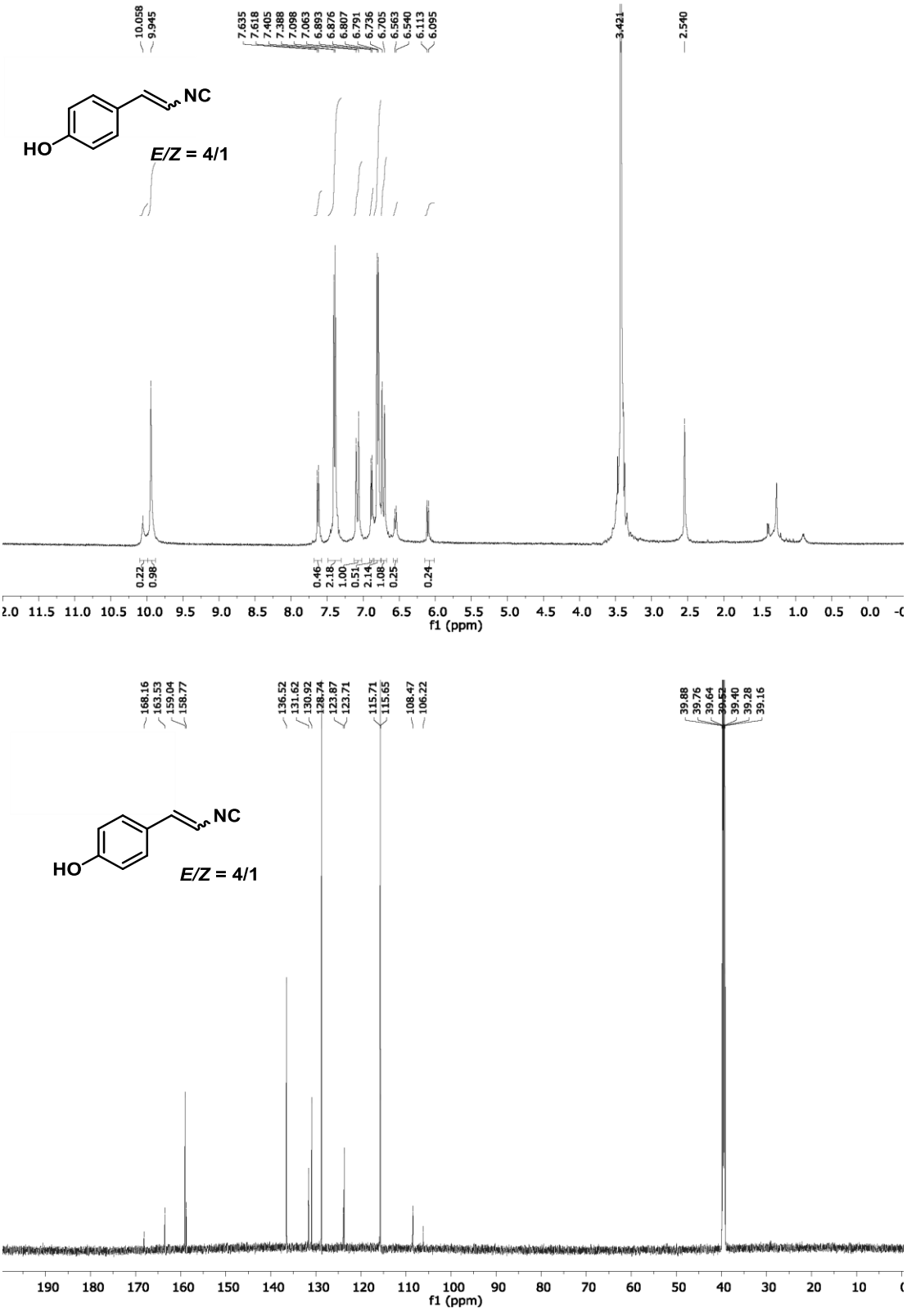


**Figure S18.** $^{1}H$ and $^{13}C$ NMR of **2**.

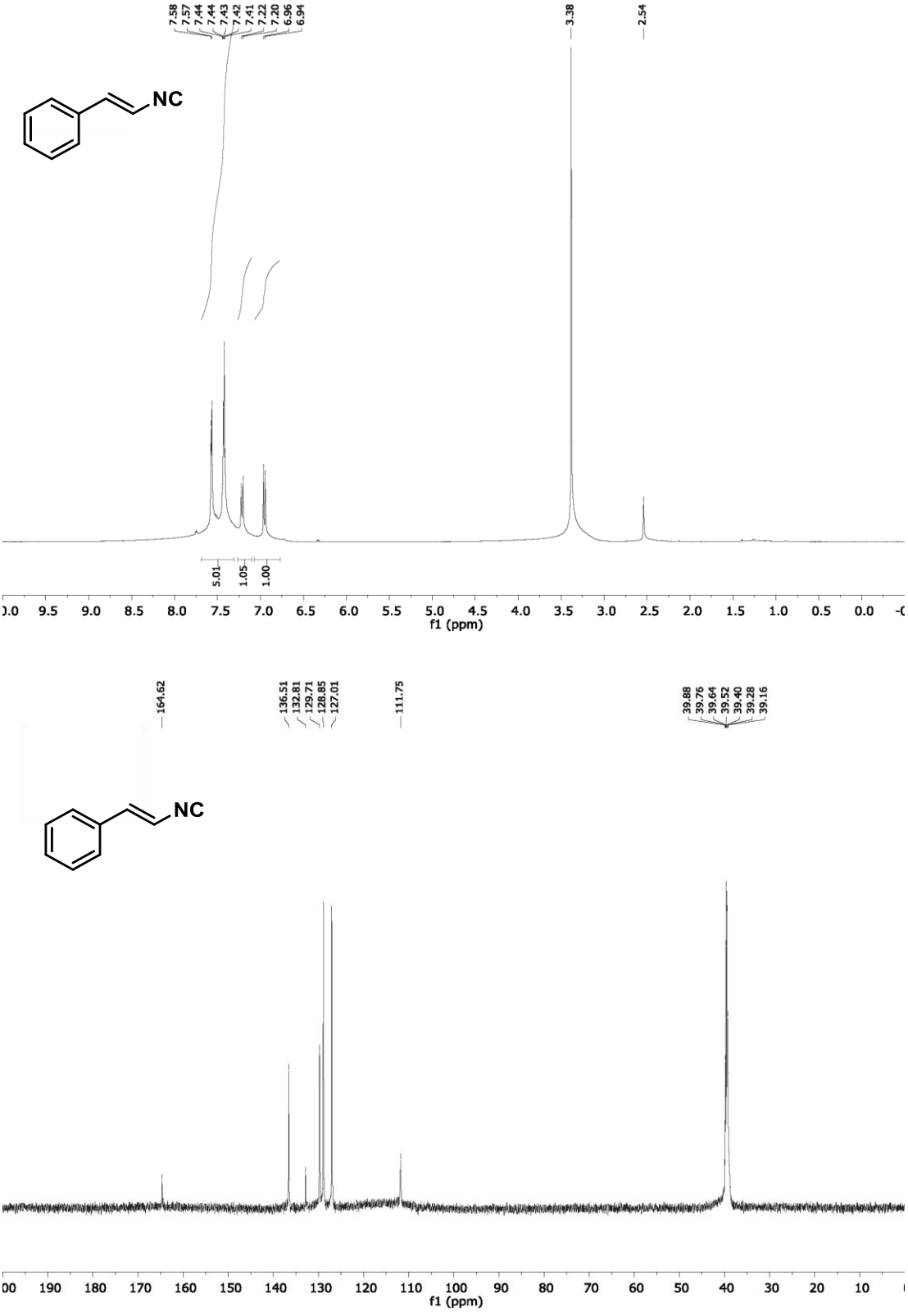


**Figure S19.** $^{1}H$ and $^{13}C$ NMR of **6**.

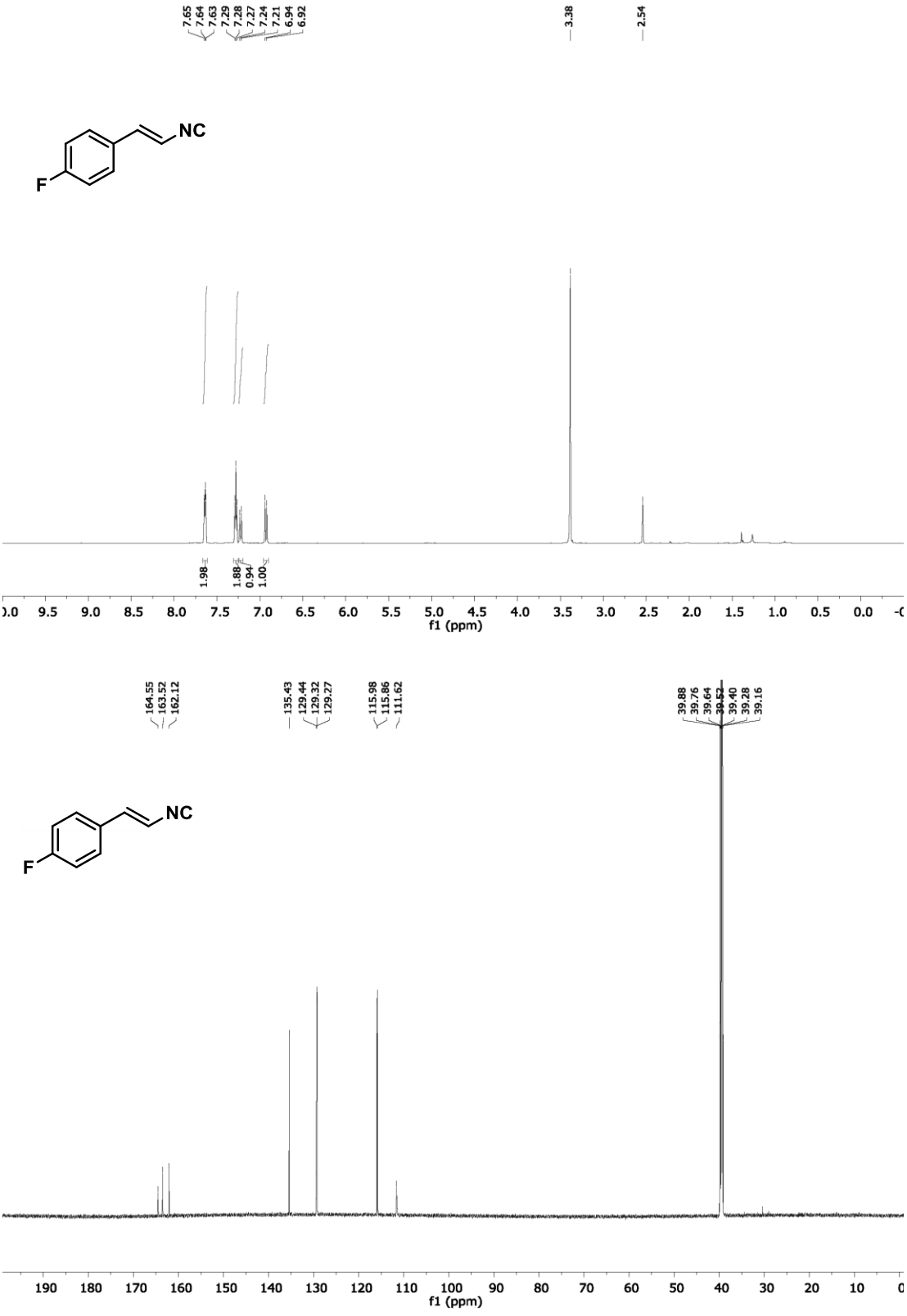


**Figure S20.** $^{1}H$ and $^{13}C$ NMR of **7**.

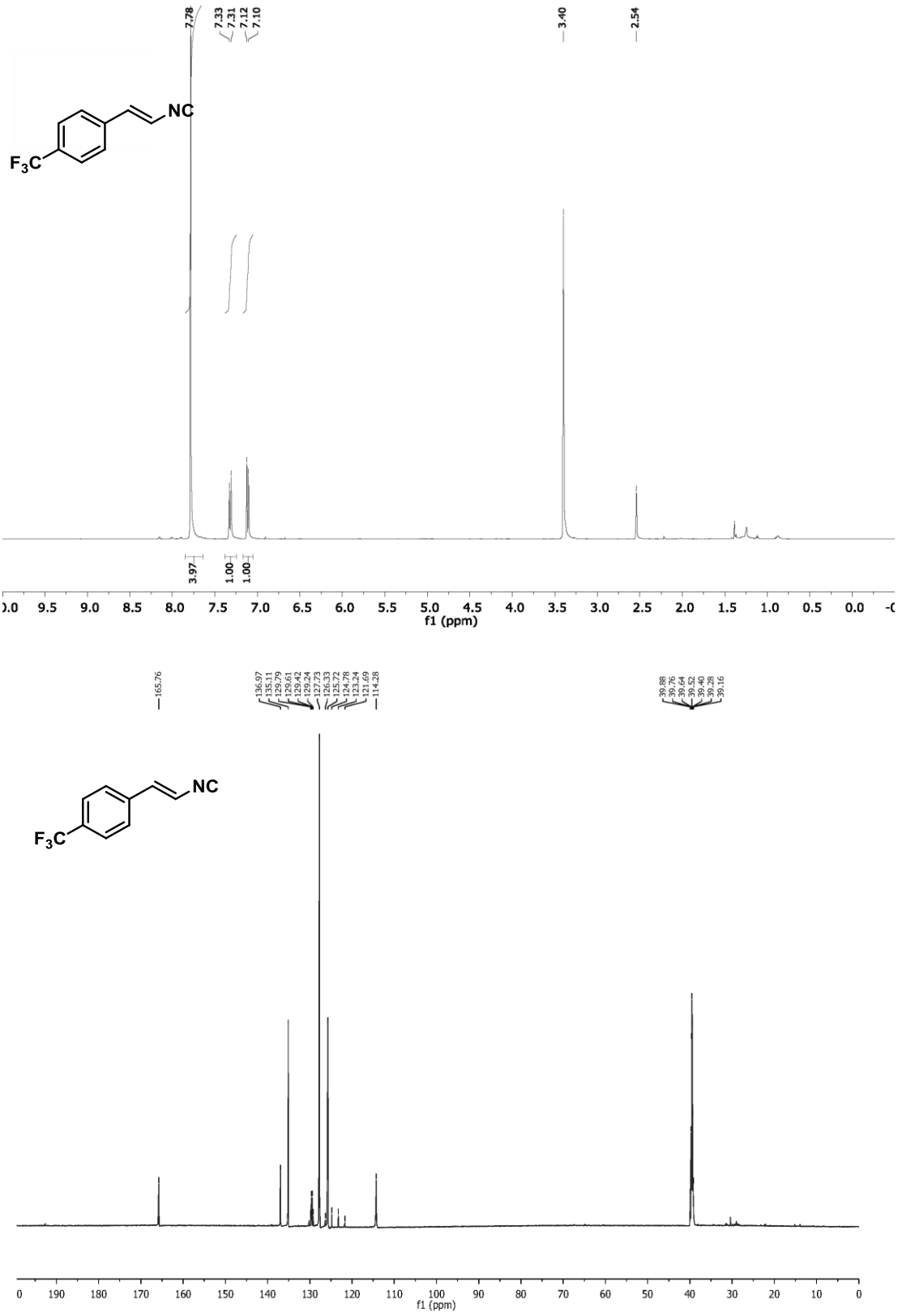


**Figure S21.** $^{1}H$ and $^{13}C$ NMR of **8**.

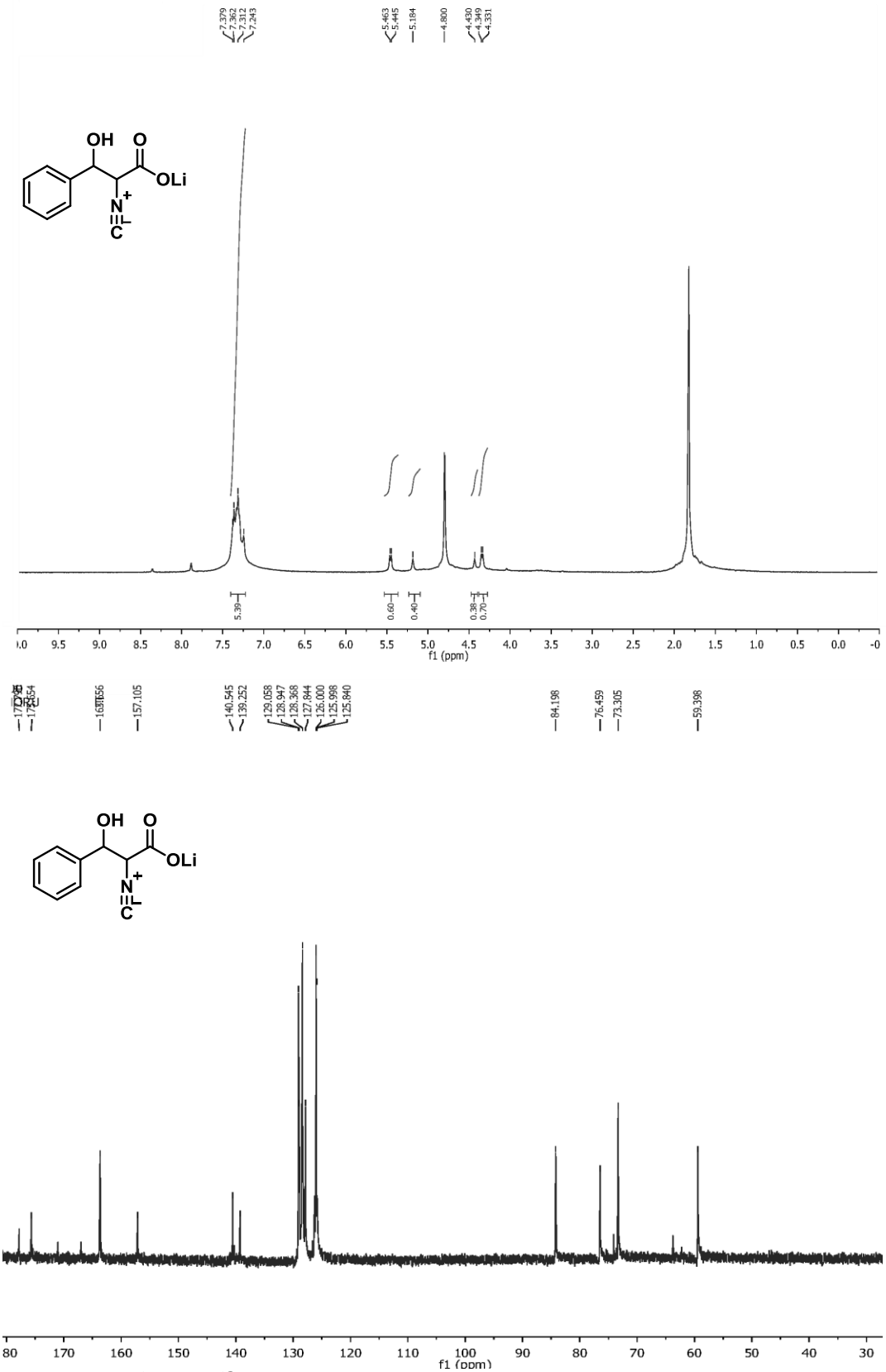


**Figure S22.** $^{1}H$ and $^{13}C$ NMR of **9**.

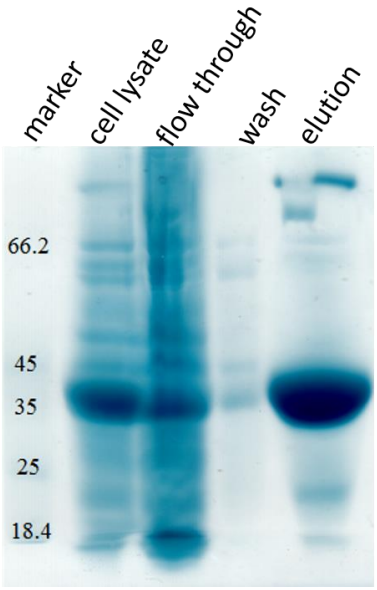


**Figure S23.** Coomassie-stained 12% SDS-PAGE analysis of N hexa-histidine-tagged IsnB. Molecular weight standards and identifications of each lane are labeled in the figure.

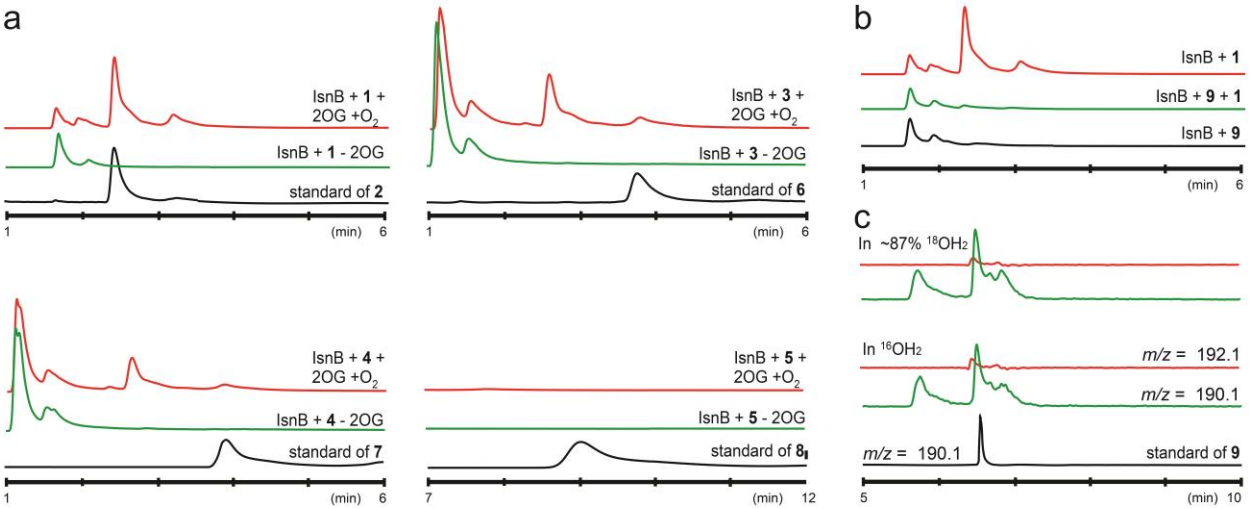


**Figure S24.** a). LC-UV chromatograms of *P*.IsnB catalyzed reaction using **1**, **3**, **4** and **5** as substrates. Comparing to the reaction using **1** as the substrate, substantial decrease of **6** and **7** production was observed. In addition, formation of **8** could not be detected. UV absorption was detected at wavelength of 266 nm. b). LC-UV chromatograms of *P*.IsnB catalyzed reaction when incubating *P*.IsnB with **9** prior to addition of **1**, $O_2$ and 2OG. The bottom, middle and top traces represent the reaction containing reconstituted *P*.IsnB with **9**, **9•1**•2OG•$O_2$, and **1**•2OG•$O_2$, respectively. After 5 mins incubation of reconstituted *P*.IsnB with **9** anaerobically, production of **2** was diminished. c). LC-MS chromatograms of *P*.IsnB catalyzed hydroxylated product **9** formation using **3** as the substrate under $^{16}OH_2$ or $^{18}OH_2$ (~ 87% $^{18}O$-enrichment) conditions. Compared to reaction conducted under $^{16}OH_2$ environment, no $^{18}O$ incorporation can be detected when $^{18}OH_2$ was used.

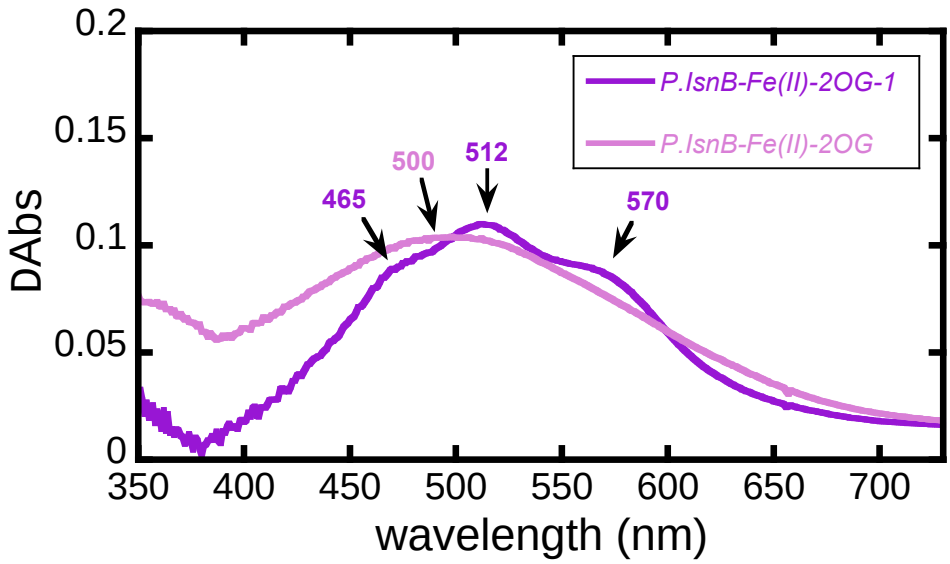


**Figure S25.** The Fe(II)-2OG MLCT band observed for the samples containing the *P*.IsnB•Fe(II)•2OG tertiary complex (pink trace) and the *P*.IsnB•Fe(II)•2OG•**1** quaternary complex (purple trace). The spectra were obtained by substrating the original spectra with the spectrum of apo *P*.IsnB. The wavelengths of the observed features are indicated in the figure. The concentrations of various species used are: P.IsnB, 0.6 mM; Fe(II), 0.54 mM; 2OG, 2.5 mM; and **1**, 1.35 mM.

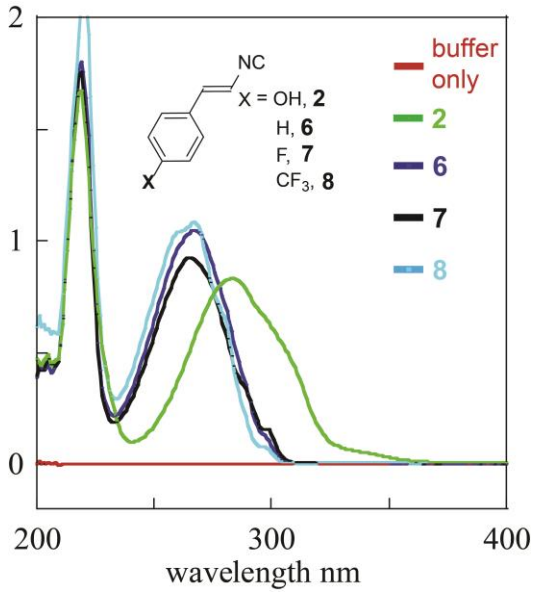


**Figure S26.** UV-Vis absorption spectra of vinyl products **2**, **6**, **7** and **8** at concentration of 50, 50, 50 and 100 μM, respectively. All compounds are dissolved in 100 mM Tris solution, pH = 7.5. Spectrum of compound **2** contains *E* and *Z* isomers in a ratio of *E*/*Z* = 4/1. The absorption of **2** at 330 nm is ~ 0.08 at concentration of 50 μM.

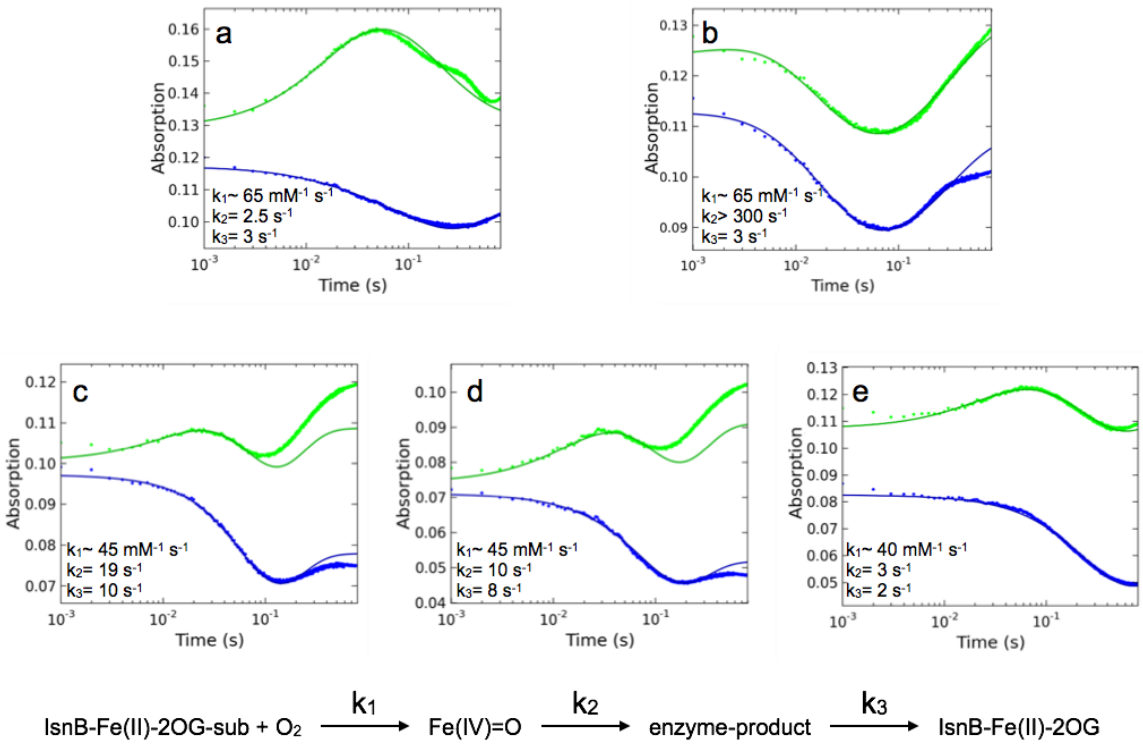


**Figure S27.** Kinetic simulations of the time dependent changes of the 440 nm (green) and the 512 nm (blue) optical features in *P*.IsnB reactions monitored by SF-Abs. (a) the result from the *P*.IsnB reaction with D-**1**; (b) the result from the *P*.IsnB reaction with **1**; (c) the result from the *P*.IsnB reaction with **3**; (d) the result from the *P*.IsnB reaction with **4**; (e) the result from the *P*.IsnB reaction with **5**. The experimental data are shown in dots and the simulations are in solid lines. The kinetic model is shown at the bottom of the figure. The rate constants for each case are listed in the corresponding plot.

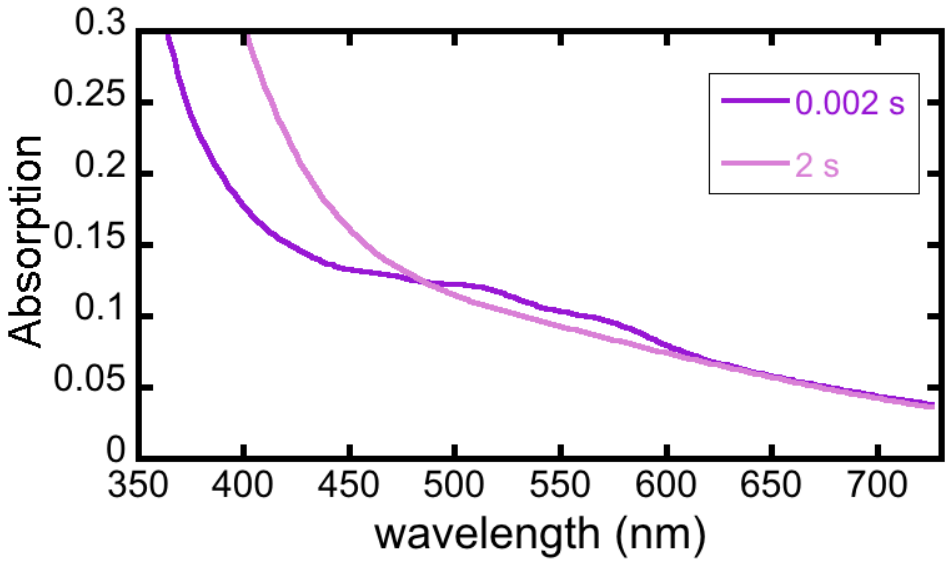


**Figure S28.** Optical spectra of *P*.IsnB taken at the beginning and the conclusion of the reaction with **1**. The concentrations of various species used are: P.IsnB, 0.3 mM; Fe(II), 0.27 mM; 2OG, 2.5 mM; **1**, 0.7 mM.

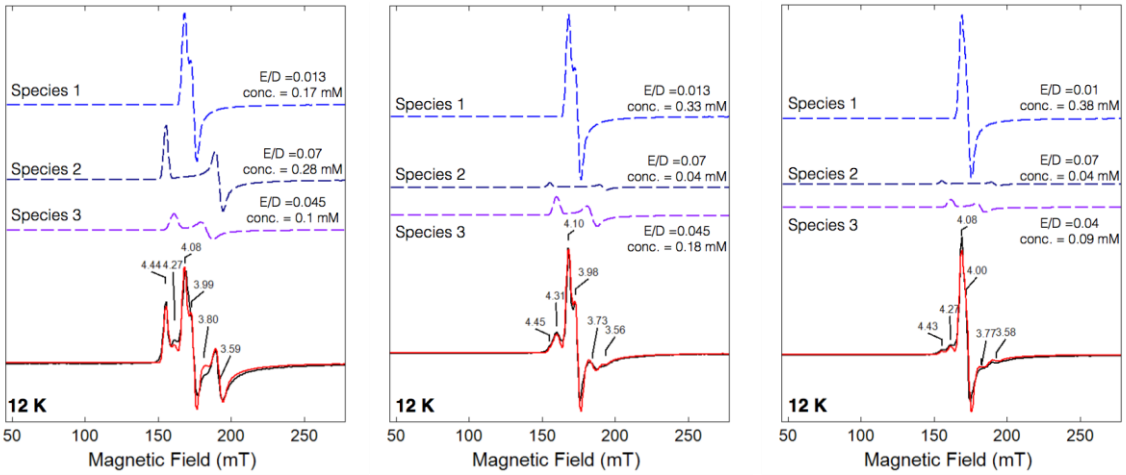


**Figure S29.** X-band (9 GHz) CW EPR spectra measured at 12 K and simulations of NO treated *P.*IsnB•Fe(II)•2OG complex (left), *P.*IsnB•Fe(II)•2OG•**1** complex (middle), and *P.*IsnB•Fe(II)•2OG•**5** complex (right). Each spectrum was found to be a superposition of three components originating from three S = 3/2 $\{FeNO\}^7$ species with different rhombicity of the zero field splitting parameter, E/D. E/D parameters and the spin concentrations of each species are listed in the figure. Black line: experimental data; Red line: overall simulations; dash lines: individual spectral components. Sample concentrations: [*P.*IsnB] = 0.6 mM, [Fe(II)] = 0.54 mM, [2OG] = 5.4 mM, [NO] = 5 mM, [**1**] or [**5**] = 2.7 mM.

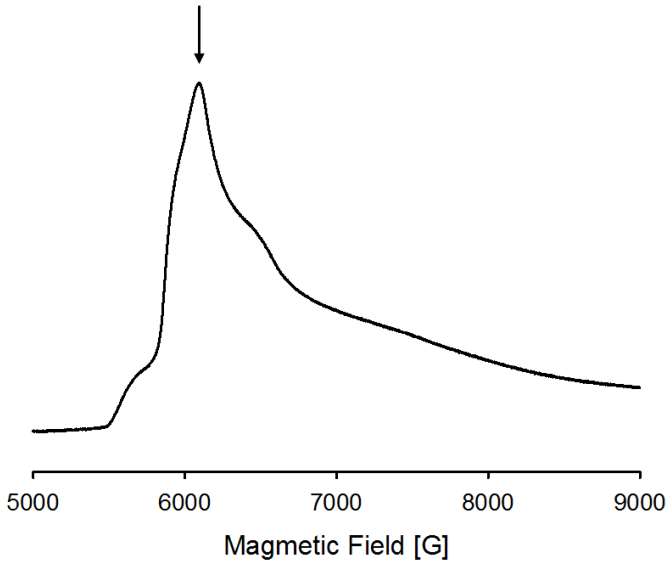


**Figure S30.** Q-band (33.6 GHz) field-swept electron spin echo (ESE) detected spectrum of NO treated *P.*IsnB•Fe(II)•2OG•D-**1** complex measured at T=3.1 K. Position of the magnetic field for the HYSCORE experiment (Fig.3) corresponds to the maximum signal at $g \approx 3.97$ and is indicated by an arrow.

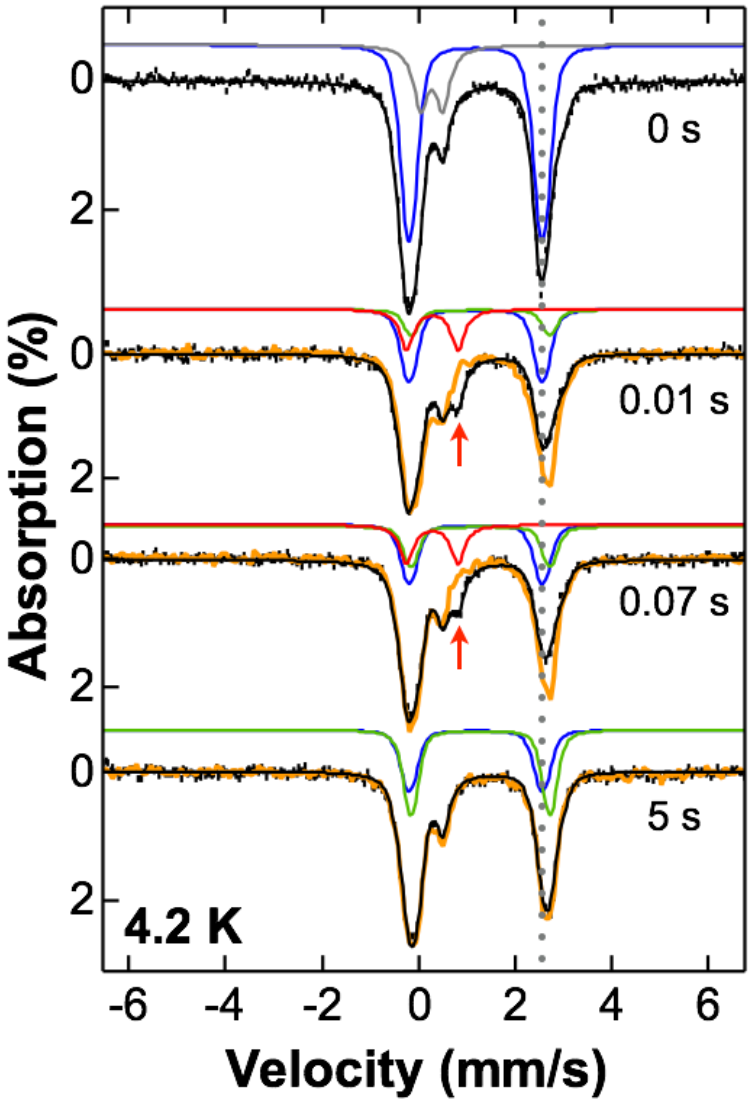


**Figure S31.** T=4.2 K zero-field Mössbauer spectra of the *P*.IsnB reaction using **1** and D-**1**. The black-hashed lines represent the spectra of samples from the reaction using D-**1** and freeze quenched at various time points indicated in the figure. The golden solid lines represent the spectra of samples from the reaction using **1** at the given quench times. The red, blue, green, and grey lines represent the spectral simulations of the Fe(IV)-oxo species, the *P*.IsnB quaternary complex, the enzyme-product and/or *P*.IsnB•Fe(II)•2OG complex, and the inactive isonitrile-Fe(II) complex, respectively. The black solid lines represent the overall simulations. The vertical dotted line indicates the position of the high energy line of the quadrupole doublet representing the *P*.IsnB•Fe(II)•2OG•**1** complex, which is clearly distinct from the position of the quadrupole doublet representing the enzyme-product and/or *P*.IsnB•Fe(II)•2OG complex. The red arrows point to the high-energy absorption line of the quadrupole doublet representing the ferryl intermediate, which are missing in the spectra generated from the samples when **1** was used in the reaction. See Table S1 and S2 for detailed spectroscopic parameters and the temperature dependent iron speciation.

**Table S1.** Mössbauer parameters of various iron species identified in this study.

| | δ (mm/s) | $\|\Delta E_Q\|$ (mm/s) | Linewidth (mm/s) |
|---|---|---|---|
| ES complex | 1.18 | 2.76 | -0.37[a] |
| EP complex / *P*.IsnB-Fe(II)-2OG complex | 1.28 | 2.84 | -0.31[a] |
| Fe(IV)-oxo | 0.29 | 1.06 | 0.35 |
| Inactive enzyme | 1.26 | 3.37 | -0.35[a] |
| Isocyano-Fe(II) complex | 0.27 | 0.47 | 0.33 |

[a] A negative linewidth represents a lineshape that is generated by a convolution of Gaussian lineshape and a Lorentzian lineshape.

**Table S2.** The relative concentrations (%) of iron species observed in FQ Mössbauer spectra.

| Time (s) | Isocyano-Fe(II) complex | ES complex | Fe(IV)-oxo | EP complex / *P*.IsnB-Fe(II)-2OG complex | Inactive enzyme |
|---|---|---|---|---|---|
| Substrate used: D-**1** | | | | | |
| 0 | 21 | 64 | 0 | 0 | 10 |
| 0.02 | 20 | 32 | 17 | 10 | 10 |
| 0.07 | 21 | 27 | 17 | 17 | 10 |
| 0.25 | 20 | 26 | 8 | 26 | 11 |
| 5 | 22 | 26 | 0 | 33 | 9 |
| Substrate used: D-**1** | | | | | |
| 0 | 20 | 67 | 0 | 0 | 13 |
| 0.02 | 28 | 39 | 0 | 27 | 10 |
| 0.07 | 24 | 34 | 0 | 32 | 10 |
| 5 | 25 | 30 | 0 | 36 | 7 |

**References:**

[1] Johnson, K. A., Simpson, Z. B., and Blom, T. (2009) Global kinetic explorer: a new computer program for dynamic simulation and fitting of kinetic data, *Anal. Biochem. 387*, 20-29.

[2] Petasis, D. T., and Hendrich, M. P. (2015) Quantitative Interpretation of Multifrequency Multimode EPR Spectra of Metal Containing Proteins, Enzymes, and Biomimetic Complexes, *Methods Enzymol. 563*, 171-208.

[3] Höfer, P., Grupp, A., Nebenführ, H., and Mehring, M. (1986) Hyperfine Sublevel Correlation (Hyscore) Spectroscopy - a 2d Electron-Spin-Resonance Investigation of the Squaric Acid Radical, *Chem. Phys. Lett. 132*, 279-282.

[4] Stoll, S., and Schweiger, A. (2006) EasySpin, a comprehensive software package for spectral simulation and analysis in EPR, *J. Magn. Reson. 178*, 42-55.

[5] Eaton, S. S., Dubach, J., Eaton, G. R., Thurman, G., and Ambruso, D. R. (1990) Electron spin echo envelope modulation evidence for carbonate binding to iron(III) and copper(II) transferrin and lactoferrin, *J. Biol. Chem. 265*, 7138-7141.

[6] Price, J. C., Barr, E. W., Tirupati, B., Bollinger, J. M., Jr., and Krebs, C. (2003) The first direct characterization of a high-valent iron intermediate in the reaction of an alpha-ketoglutarate-dependent dioxygenase: a high-spin FeIV complex in taurine/alpha-ketoglutarate dioxygenase (TauD) from Escherichia coli, *Biochemistry 42*, 7497-7508.

[7] Matthews, M. L., Krest, C. M., Barr, E. W., Vaillancourt, F. H., Walsh, C. T., Green, M. T., Krebs, C., and Bollinger, J. M. (2009) Substrate-triggered formation and remarkable stability of the C-H bond-cleaving chloroferryl intermediate in the aliphatic halogenase, SyrB2, *Biochemistry 48*, 4331-4343.

[8] Srnec, M., Wong, S. D., Matthews, M. L., Krebs, C., Bollinger, J. M., Jr., and Solomon, E. I. (2016) Electronic Structure of the Ferryl Intermediate in the alpha-Ketoglutarate Dependent Non-Heme Iron Halogenase SyrB2: Contributions to H Atom Abstraction Reactivity, *J. Am. Chem. Soc. 138*, 5110-5122.

[9] Huang, J. L., Tang, Y., Yu, C. P., Sanyal, D., Jia, X., Liu, X., Guo, Y., and Chang, W.-c. (2018) Mechanistic Investigation of Oxidative Decarboxylation Catalyzed by Two Iron(II)- and 2-Oxoglutarate-Dependent Enzymes, *Biochemistry 57*, 1838-1841.

[10] Chang, W.-c., Li, J., Lee, J. L., Cronican, A. A., and Guo, Y. (2016) Mechanistic Investigation of a Non-Heme Iron Enzyme Catalyzed Epoxidation in (-)-4'-Methoxycyclopenin Biosynthesis, *J. Am. Chem. Soc. 138*, 10390-10393.

[11] Chang, W.-c., Guo, Y., Wang, C., Butch S. E., Rosenzweig, A. C., Boal, A. K., Krebs. C., Bollinger, J. M. Jr. (2014) Mechanism of the C5 stereoinversion reaction in the biosynthesis of carbapenem antibiotics, *Science*, *343*, 1140-1144.